Journal of Environmental Chemical Engineering 12 (2024) 113424

Contents lists available at ScienceDirect

Journal of Environmental Chemical Engineering

journal homepage: www.elsevier.com/locate/jece

Selective electrochemical oxidation of organic compounds in a mass transfer-enhanced electrochemical flow reactor (e^-NETmix)

Clarissa H. Rosa [a,b,c,1], Daniela F.S. Morais [b,c,1], Gilber R. Rosa [a], João H.Z. dos Santos [d], José Carlos B. Lopes [b,c,e], Madalena M. Dias [b,c], Rosa Montes [f], Rosario Rodil [f], José Benito Quintana [f], Gabriel Antonio Cerrón-Calle [b,c,g], Sergi Garcia-Segura [g], Carlos J. Tavares [h], Vítor J.P. Vilar [b,c,*], Francisca C. Moreira [b,c,*]

[a] Escola de Química e Alimentos, Universidade Federal do Rio Grande, Campus Santo Antônio da Patrulha, Rua Barão do Cahy 125, Cidade Alta, Santo Antônio da Patrulha, RS 95500-000, Brazil
[b] LSRE-LCM – Laboratory of Separation and Reaction Engineering - Laboratory of Catalysis and Materials, Faculty of Engineering, University of Porto, Rua Dr. Roberto Frias, Porto 4200-465, Portugal
[c] ALiCE – Associate Laboratory in Chemical Engineering, Faculty of Engineering, University of Porto, Rua Dr. Roberto Frias, Porto 4200-465, Portugal
[d] Instituto de Química, Universidade Federal do Rio Grande do Sul, Av. Bento Gonçalves 9500, Porto Alegre, RS 91501-970, Brazil
[e] CoLAB NET4CO2, Rua Júlio de Matos, 828-882, Porto 4200-355, Portugal
[f] Aquatic One Health Research Center (ARCUS) & Department of Analytical Chemistry, Nutrition and Food Chemistry, Universidade de Santiago de Compostela, R. Constantino Candeira, IIAA building, Santiago de Compostela, Galicia 15782, Spain
[g] Nanosystems Engineering Research Center for Nanotechnology-Enabled Water Treatment, School of Sustainable Engineering and the Built Environment, Arizona State University, Tempe, AZ 85287-3005, USA
[h] CF-UM-UP – Centre of Physics of the Universities of Minho and Porto, University of Minho, Guimarães 4804-533, Portugal

ARTICLE INFO

Keywords:
Anodic oxidation
Electrocatalysis
Value-added products
Microreactor
Reactor design
Static mixer

ABSTRACT

e^-NETmix stands as an electrochemical flow reactor engineered to enhance mass transfer. This study aimed at assessing the performance of the e^-NETmix reactor in the realm of organic electrosynthesis. Specifically, the research focused on the selective electrochemical oxidation of 4-methoxybenzyl alcohol (4-MBA) to *p*-anisaldehyde (PAA) using a bare fluorine-doped tin oxide (FTO) anode. The efficiency of the process was assessed for distinct current densities (*j*), Reynolds numbers (*Re*), supporting electrolyte contents, and substrate initial contents. The e^-NETmix reactor was extensively compared to a commercial electrochemical flow reactor (MicroFlowCell from ElectroCell, Denmark). e^-NETmix facilitated the use of a broader range of *j* (0.8–2.0 mA cm^{-2} *versus* 0.8 mA cm^{-2}) together with smaller *Re* (≥190 *versus* >1750), supporting electrolyte contents (≥1 mM *versus* ≥30 mM), and substrate initial contents (≥2.0 mM *versus* ≥3.0 mM) with no loss of PAA production or energy consumption. These findings underscore a remarkable suitability of e^-NETmix as a reactor for organic electrosynthesis.

1. Introduction

Typically, organic electrosynthesis occurs through inner sphere reactions close to the electrode surface. In the case of processes driven by oxidation reactions, the electrosynthesis takes place on the anode surface. One or more substrates are transferred from the bulk liquid phase to the anode surface, where they are adsorbed (S_{ads}). Afterward, the oxidation of the substrate(s) occurs by direct charge transfer (Eq. (1) [1]) or action of reactive oxygen species (ROS) generated on the anode surface. One or more adsorbed products (P_{ads}) are formed in both cases. Ultimately, the P_{ads} should desorb from the anode surface and be transferred to the bulk liquid phase to avoid overoxidation [1–3].

$$S_{ads} \rightarrow P_{ads} + ae^- \quad (1)$$

Given this surface-driven reaction mechanism, it is easy to infer that mass transfer is critical in organic electrosynthesis. Therefore, various

* Corresponding authors at: LSRE-LCM – Laboratory of Separation and Reaction Engineering - Laboratory of Catalysis and Materials, Faculty of Engineering, University of Porto, Rua Dr. Roberto Frias, Porto 4200-465, Portugal.
E-mail addresses: vilar@fe.up.pt (V.J.P. Vilar), francisca.moreira@fe.up.pt (F.C. Moreira).
[1] The first two authors contributed equally to this work.

https://doi.org/10.1016/j.jece.2024.113424

Available online 29 June 2024
2213-3437/© 2024 The Author(s). Published by Elsevier Ltd. This is an open access article under the CC BY-NC-ND license (http://creativecommons.org/licenses/by-nc-nd/4.0/).

efforts have been made to address mass transfer limitations in electrochemical reactors. In this context, electrochemical flow reactors have become very popular since they provide enhanced mass transfer and, in addition, increased heat transfer, energy performance, scalability, process safety, automation, and reproducibility. The most common electrochemical flow reactors refer to parallel plate flow reactors/cells, also known as filter-press electrochemical reactors/cells. A summary of these reactors is provided elsewhere [4–6]. For instance, Selt et al. [7] conducted electrochemical synthesis of biphenols from phenols with higher productivity and yield in a flow electrolysis cell (productivity of 0.3–1.3 g min^{-1} and yield of 58–62 %) compared to a beaker-type batch cell (productivity of 2 mg min^{-1} and yield of 46 %).

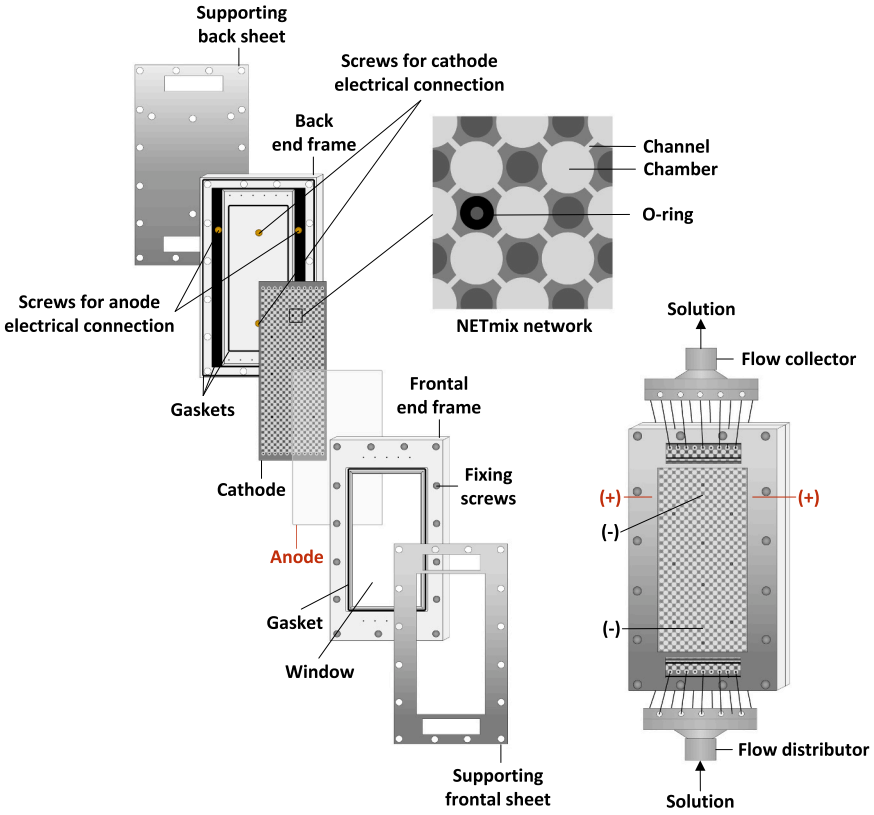

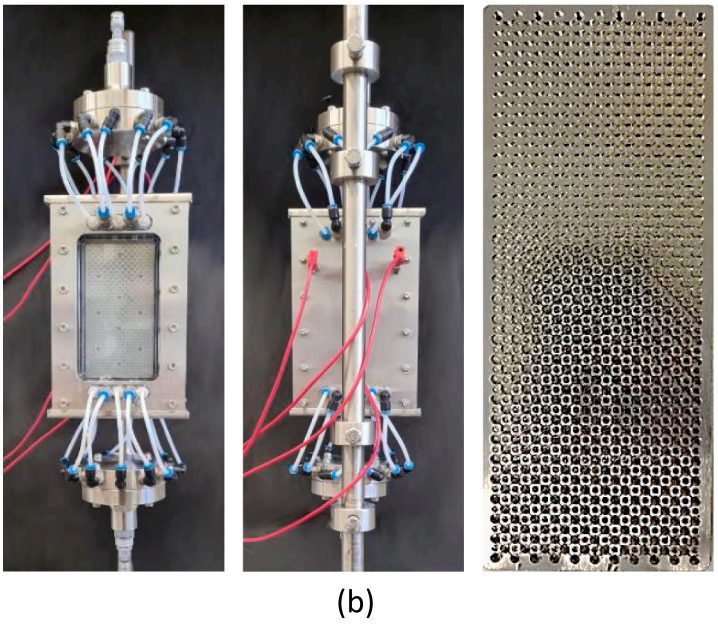

Fig. 1. (a) Sketches of the e^{-}NETmix reactor disassembled (left) and assembled (right) (frontal views), and (b) pictures of the e^{-}NETmix reactor assembled (left – frontal view; center – back view) and picture of the electrode plate with the NETmix engraved (right). The e^{-}NETmix reactor is equipped with a bare fluorine-doped tin oxide (FTO) glass anode.

A novel parallel plate flow reactor – named e^-NETmix – was developed recently. This reactor comprises a fluid distributor network – based on the NETmix technology – composed of cylindrical chambers interconnected by prismatic channels arranged at a 45º angle with the chamber axis and a 90º angle with neighboring channels. A provisional patent application on this electrochemical flow reactor was recently filled, encompassing distinct reactor configurations [8]. One possible configuration of the e^-NETmix reactor is fully presented in Morais et al. [9] and characterized regarding mass transfer. In this e^-NETmix configuration, illustrated in Fig. 1, the NETmix network is engraved on a plate working as an electrode and covered by a flat plate electrode. The plate on which the NETmix network is machined is made of stainless-steel, while the flat plate electrode can be interchangeable with materials of different natures. The NETmix network has chambers with a diameter of 3.25 mm and channels with a length of 0.99 mm and a width of 0.60 mm. The chambers and channels depth is 1.50 mm. Given the micro dimensions of the channels, the e^-NETmix reactor can be classified as a microreactor. The use of microfluidic reactors for organic electrosynthesis is not new. The high electrode surface area-to-volume and short interelectrode distance are key advantages of these devices [10]. Review articles focused on organic electrosynthesis using microreactor technology have been published [11,12], covering a multitude of microreactors. For example, Nöel and co-workers designed an undivided filter-press electrochemical flow microreactor with an 8-channel configuration (106×3 mm per channel) and an interelectrode gap of 0.25–0.50 mm [13]. Furthermore, Wirth and colleagues developed an electrochemical flow microreactor featuring a serpentine flow channel (3 mm with) and an interelectrode gap of 0.25 mm [14].

Morais et al. [9] reports volumetric mass transfer coefficients (k_mA) from (1.29±0.03)×10^{-1} s^{-1} to (5.10±0.07)×10^{-1} s^{-1} and mass transfer coefficients (k_m) from (6.78±0.02)×10^{-5} m s^{-1} to (2.68±0.04)×10^{-4} m s^{-1} in e^-NETmix for Reynolds numbers (*Re*) from 100 to 1750 and corresponding mean linear fluid velocities (ν_{avg}) from 0.10 m s^{-1} to 1.82 m s^{-1}. The k_mA and k_m values are up to ~54-fold and ~24-fold higher than those given in various lab-assembled and commercial electrochemical flow reactors mentioned in the literature (references provided in [8]) for identical ν_{avg} and *Re* conditions, respectively. Furthermore, a detailed comparison with a Micro Flow Cell from ElectroCell A/S (Denmark) revealed larger k_mA and k_m values of ~63-fold and ~8.6-fold, respectively, in e^-NETmix for similar *Re*. The superior mass transfer performance of the e^-NETmix device is unquestionable and mainly attributed to the NETmix network, which induces convective mixing and the development of a laminar chaotic flow regime.

The current study covers the validation of the e^-NETmix reactor developed in Morais et al. [9] for organic electrosynthesis. The selective oxidation of the primary alcohol 4-methoxybenzyl alcohol (4-MBA) to its aldehyde *p*-anisaldehyde (PAA) is the model synthesis reaction under evaluation. PAA is widely used as a flavor and a fragrance in the food, personal care, and pharmaceutical industries. Current industrial routes of PAA synthesis cause severe environmental problems as they mainly involve the oxidation of *p*-cresyl methyl ether by manganese dioxide in acidic media or the methylation of *p*-cresol or anisole in organic solvents and harsh conditions of pressure and temperature [15,16]. Electrosynthesis using mild conditions, i.e., ambient temperature and pressure, neutral pH, and aqueous media (organic solvent-free), is a more sustainable alternative. The 4-MBA conversion to PAA by electrochemical oxidation has been studied [17–21], as well as by photoelectrocatalysis and photocatalysis [22–25]. The efficiency of the 4-MBA selective oxidation to PAA is evaluated for different current densities (*j*), hydrodynamic conditions (in terms of *Re*), supporting electrolyte contents, and 4-MBA initial contents. The e^-NETmix reactor is thoroughly compared with the Micro Flow Cell from ElectroCell A/S (Denmark), referred to as e^-Cell for simplification purposes. A bare fluorine-doped tin oxide (FTO) glass electrode is used as the anode. FTO is transparent, highly conductive, thermostable, and resistant to strong acids and bases, as well as organic solvents [26]. Surface-modified FTO electrodes have been extensively used in solar cells [27,28] and electrochemical sensors [29,30]. To the authors' knowledge, the use of bare FTO for organics oxidation is scarce. However, it has already demonstrated its ability to catalyze the electrochemical oxidation of certain organic compounds [31,32].

2. Material and methods

2.1. Chemicals

Chemicals are provided in the Supplementary Material file.

2.2. Electrochemical reactors

2.2.1. Lab-assembled electrochemical flow reactor: e^-NETmix

The e^-NETmix experimental set-up, represented in Fig. 1, is described in detail in Morais et al. [9]. It is mainly composed of (i) a 316-grade stainless-steel plate with an engraved NETmix network working as an electrode, (ii) a flat plate made of any preferred material working as an electrode, (iii) polyethylene terephthalate (PET) end frames to hold the components together and seal the reactor by mechanical compression, (iv) stainless-steel supporting sheets to give resistance to the end frames, and (v) various gaskets and O-rings to avoid leakages and electrodes shortcut. The fluid flows upwards within the NETmix network, which acts as a static mixer. The NETmix network is created by the repetition of a unit cell in which a cylindrical chamber is connected to four prismatic channels positioned at a 45º angle with the chamber axis, originating a 90º angle between neighboring channels. Chambers exhibit 3.25 mm diameter (*D*) and 1.50 mm depth (ω), while channels show 0.99 mm length (*L*), 0.60 mm width (*d*), and 1.50 mm ω. The interelectrode gap is assumed to range from ~0 mm at the ends of the NETmix lateral walls to ~1.5 mm (NETmix depth) at the NETmix base. Chambers are distributed by 55 rows, each row alternating between 10 and 11 columns of chambers. There is a total of 578 chambers and 1080 channels connected to the chambers, of which 525 chambers and 1000 channels are covered by the flat plate electrode. This translates to a total volume of 8.2 mL, with 7.4 mL in direct contact with both the anode and the cathode, constituting the active volume. The active surface area of the flat plate electrode is 49.5 cm^2, while the active surface area of the NETmix plate electrode is 141.6 cm^2. The fluid enters the reactor through 11 inlet chambers at the bottom of the network and exits via 11 outlet chambers at the top of the network. The pressure drop in the e^-NETmix reactor may vary from >0.5 kPa to >17 kPa for water at 25 ºC and *Re* from 100 to 1150, based on estimates derived from the data presented by Fonte et al. [33].

In the current application, the stainless-steel plate with the NETmix network works as a cathode. The anode consists of a flat glass plate of 3.2 mm thickness one-side coated with a thin transparent film of FTO, exhibiting ~150 nm thickness, 10 Ω sq^{-1} resistance, and a transmittance >80 %, supplied by Dyenamo (Sweden). The glass plate substrate is made of standard sodium glass, containing ~70 % silicon dioxide (SiO_2), ~13 % sodium oxide (Na_2O), ~7 % calcium oxide (CaO), among other minor constituents. The bare FTO anode was utilized in its original condition. The selection of FTO as the anode stemmed from preliminary tests involving various electrode materials, with FTO consistently demonstrating superior efficiencies.

2.2.2. Commercial electrochemical flow cell: e^-Cell

The MicroFlowCell from ElectroCell (Denmark), e^-Cell, is also described in detail in Morais et al. [9] and is represented in Figure SM-1. It is mainly composed of (i) two flat plates working as the electrodes (an anode and a cathode), (ii) a polytetrafluoroethylene (PTFE) flow frame with a trapezoid-shaped channel filled with a turbulence promoter (TP) mesh with 80 % porosity made of polypropylene (PP), (iii) PTFE end frames to hold the components together and seal the reactor by mechanical compression, (iv) stainless-steel supporting sheets to give

resistance to the end frames, and (v) peroxide-cured ethylene propylene diene monomer (EPDM) gaskets between all the cell components to avoid leakages. The fluid flows in the trapezoid-shaped channel of the flow frame. A rectangular section of the trapezoid of 33.3 mm *L*, 30.0 mm *d*, and 3.8 mm ω is in contact with the electrodes, originating an electrodes' active surface area of 10 cm^2. The interelectrode gap is 3.8 mm. The fluid enters the e^-Cell reactor through a single bottom inlet and leaves the reactor through a single top outlet. The anode is a glass flat plate one-side coated with a thin transparent FTO film equal to that used in e^-NETmix (see Section 2.2.1). The cathode is a 316-grade stainless-steel flat plate.

2.3. Electrochemical system

Both the e^-NETmix and the e^-Cell reactors were integrated in an electrochemical system mainly composed of: (i) a cylindrical glass vessel magnetically stirred and thermostatically controlled with the aid of a refrigerated heating circulating bath (Grant, model ecocool 150 R) to ensure proper homogenization and temperature control of the solution, (ii) a gear pump (Ismatec, model BVP-Z, with Ismatec Z-142 or Z-040 pump head), and (iii) a power supply (Velleman®, model LABPS3005DN, 0–5 A, 0–30 V). All the system components were connected by PTFE tubing. Full details of this system are given in Morais et al. [9].

2.4. Electrochemical characterization of the FTO anode

Electrochemical characterization of the commercial FTO anode was conducted by cyclic voltammetry (CV) using a potentiostat PGSTAT302N (Metrohm, USA). An undivided and thermostatically controlled batch cell under magnetic stirring at 300 rpm was used together with a standard three-electrode cell configuration. The FTO was the working electrode, a platinum coil was the auxiliary electrode, and a silver/silver chloride (Ag/AgCl) (3.2 M) was the reference electrode. A volume of 50 mL of a solution composed of ultrapure water with 100 mM Na_2SO_4 as the supporting electrolyte in the presence or absence of 4-MBA at different concentrations (1.0–10 mM) was used. CV measurements were performed at 25±1 ºC at a scan rate of 10 mV s^{-1} ranging from 0 V to 1.4 V *vs.* Ag/AgCl.

2.5. Selective electrochemical oxidation of 4-MBA to PAA

The electrochemical system was operated in semi-batch mode, i.e., the solution was constantly recirculated between e^-NETmix or e^-Cell devices and the homogenization vessel. The substrate solution was prepared by spiking ultrapure water with 0.25–3.0 mM 4-MBA in the absence or presence of 0.1–100 mM Na_2SO_4 as the supporting electrolyte. A 500 mL or 101 mL solution volume in e^-NETmix or e^-Cell, respectively, was placed into the homogenization vessel. The volume of solution was different in the two reactors to guarantee the same ratio of anode active surface area to solution volume (9.9 m^2 m^{-3}) since the process efficiency is directly related to this ratio. First, the solution was recirculated through the system until it reached a temperature of 25±1 ºC (~10–15 min). Afterward, the solution pH was adjusted to 7.0±0.2 (neutral pH) and recirculated for 10 min to provide its homogenization. The solution flowed at 6.7–118.0 L h^{-1} (e^-NETmix) or 4.3–75.5 L h^{-1} (e^-Cell), giving rise to *Re* in the range 100–1750, corresponding to the minimum and maximum permissible values in e^-Cell. The e^-NETmix reactor can operate within the entire laminar flow regime range, with a flow rate of 135 L h^{-1} for a *Re* of 2000, resulting in a processing capacity of 3240 L per day. A control sample was taken before the beginning of the reactions, which was marked by the switching on of the power supply at a constant *j* in the range 0.3–3.0 mA cm^{-2}. The solution temperature and pH were continuously measured and adjusted to maintain the initial values throughout the reaction time. Samples were taken at predetermined time intervals up to 120 min of reaction. Experiments were carried out in duplicate.

The efficiency of the 4-MBA selective oxidation to PAA was assessed in terms of conversion, 4-MBA initial oxidation rate ($r_{0,4\text{-MBA}}$), selectivity to PAA, yield to PAA, PAA production rate, current efficiency (CE), energy consumption for electrical current supply (EC), material recovery (MR), and consumed charge. For some experiments, the generated by-products were also assessed.

The conversion (in %) was given by the amount of substrate (4-MBA) converted per amount of substrate fed – see Eq. (2) [34].

$$\text{Conversion} = \frac{[\text{4-MBA}]_0 - [\text{4-MBA}]_t}{[\text{4-MBA}]_0} \times 100 \quad (2)$$

where $[\text{4-MBA}]_0$ is the initial concentration of 4-MBA in solution (in mM) and $[\text{4-MBA}]_t$ is the concentration of 4-MBA in solution at a given reaction time *t* (in mM).

The $r_{0,4\text{-MBA}}$ (in mM min^{-1}) was calculated according to Eq. (3), considering the pseudo-first-order kinetic constant for 4-MBA oxidation ($k_{4\text{-MBA}}$, in min^{-1}). The $k_{4\text{-MBA}}$ was determined by the pseudo-first-order kinetic model represented in Eq. (4).

$$r_{0,4\text{-MBA}} = k_{4\text{-MBA}} \times [\text{4-MBA}]_0 \quad (3)$$

$$[\text{4-MBA}]_t = [\text{4-MBA}]_0 \times e^{-k_{4\text{-MBA}} \times t} \quad (4)$$

where $[\text{4-MBA}]_t$ and $[\text{4-MBA}]_0$ are in mM and *t* is the reaction time (in min).

A non-linear regression method was applied to fit the pseudo-first-order kinetic model to the experimental data using Fig.P software from Biosoft. The goodness of fit was assessed through the relative standard deviations, residual variance (S_R^2), and coefficient of determination (R^2).

The selectivity to PAA (in %) corresponded to the amount of PAA (product) formed per total amount of 4-MBA (substrate) converted – see Eq. (5) [34].

$$\text{Selectivity to PAA} = \frac{[\text{PAA}]_t}{[\text{4-MBA}]_0 - [\text{4-MBA}]_t} \times 100 \quad (5)$$

where $[\text{PAA}]_t$ is the content of PAA in solution at a given reaction time *t* and all variables are in mM.

The yield to PAA (%) corresponded to the amount of PAA (product) formed per total amount of PAA that could be formed – see Eq. (6) [34].

$$\text{Yield to PAA} = \frac{[\text{PAA}]_t}{[\text{4-MBA}]_0} \times 100 \text{ or}$$
$$\text{Yield to PAA} = \text{Conversion} \times \text{Selectivity to PAA} \quad (6)$$

where $[\text{PAA}]_t$ and $[\text{4-MBA}]_0$ are in mM.

The PAA production rate (in mM min^{-1}) was determined according to Eq. (7):

$$\text{PAA production rate} = r_{0,4\text{-MBA}} \times \text{Selectivity to PAA} \quad (7)$$

where $r_{0,4\text{-MBA}}$ is in mM min^{-1}.

The CE (in %), also called Faraday efficiency, was calculated according to Eq. (8) [35]:

$$\text{CE} = \frac{n \times F \times [\text{PAA}]_t \times V_s}{I \times t} \times 100 \quad (8)$$

where *n* is the theoretical number of electrons exchanged in the elementary act of the electrode reaction (two exchanged electrons per PAA molecule – see Section 3.1), *F* is the Faraday constant (96485 C mol^{-1}), $[\text{PAA}]_t$ is in M, V_s is the solution volume in the system (in L), *I* is the applied current (in A), and *t* is in s.

The EC (in kWh mol^{-1}) was calculated in terms of specific energy consumption per unit product mass via Eq. (9) [36]:

$$EC = \frac{E_{cell} \times I \times t}{V_s \times [PAA]_t \times 1000} \quad (9)$$

where E_{cell} is the average cell potential (in V), I is in A, t is in h, V_s is in L, $[PAA]_t$ is in M, and 1000 is a unit conversion factor.

The MR (in %), defined as the relative amount of products of interest (PAA in this case) and substrate (4-MBA) in solution, was calculated via Eq. (10):

$$MR = \frac{[PAA]_t + [4\text{-MBA}]_t}{[4\text{-MBA}]_0} \times 100 \quad (10)$$

where all variables are in mM.

The consumed specific charge (in Ah L^{-1}) was calculated according to Eq. (11) [35]:

$$\text{Consumed specific charge} = \frac{I \times t}{V_s} \quad (11)$$

where I is A, t is in h, and V_s is in L.

The by-products were evaluated in the first instance by liquid chromatography-quadrupole time-of-flight tandem mass spectrometry (LC-QTOF-MS/MS) and afterward by high-performance liquid chromatography (HPLC). The carbon dioxide (CO_2) was quantified by performing a carbon balance, in which the dissolved organic carbon (DOC) was measured, and it was assumed that the difference between the DOC of the initial solution and of a given sample was entirely due to the CO_2 production.

Parameters were computed based on a fixed 4-MBA conversion of 50 % and for 120 min of reaction (total reaction time). A 4-MBA conversion of 50 % was chosen as it reflects the maximum conversion attained after 120 min of reaction in the experiment with the lower 4-MBA oxidation rate, corresponding to the trial at *Re* of 100 in the e^-Cell reactor (see Tables 1 and 2). This approach enables direct comparison of all experiments. Data was also computed for 120 min of reaction as it resulted in higher conversion values in most of the experiments, typically >95 % in e^-NETmix and >60 % in e^-Cell, thereby enhancing the discussion of results.

2.6. Analysis of variance

A four-way analysis of variance (ANOVA) was conducted to assess the influence of four operational parameters (*j*, *Re*, $[Na_2SO_4]$, and $[4\text{-MBA}]_0$) on both $r_{0,4\text{-MBA}}$ and PAA selectivity separately. Each reactor underwent individual analysis. The reactors, e^-Cell and e^-NETmix, were treated as independent variables, while *j*, *Re*, $[Na_2SO_4]$, and $[4\text{-MBA}]_0$ were considered dependent variables. *p*-value, F-value, and significance levels were evaluated to ascertain the statistical significance of the findings. All statistical analyses were performed using R Studio.

2.7. Analytical determinations

4-MBA, PAA, and 4-MBZA contents were followed by reversed-phase HPLC using a VWR-Hitachi LaChrom Elite® liquid chromatograph. This equipment was fitted with a Merck LiChrospher® 100 RP-18 (5 μm) LiChroCART® 125–4 column at 25 °C and a diode array detector (DAD) set at a wavelength of 225 nm. Samples of 40 μL were injected. For the determination of 4-MBA and PAA, the mobile phase was composed of a mixture of 55:22.5:22.5 (% v/v) of 0.010 M oxalic acid:methanol: acetonitrile (eluents A:B:C) flowing at 0.7 mL min^{-1}. The run time was 8 min, and the retention time was 3.6 min for 4-MBA and 6.4 min for PAA. The quantification and detection limits were 0.2 μM and 0.06 μM for 4-MBA, respectively, and 0.6 μM and 0.2 μM for PAA, respectively. For the determination of 4-MBZA, the mobile phase was composed of a mixture of 40:30:30 (% v/v) of eluents A:B:C flowing at 1.0 mL min^{-1}. The run time was 3.5 min, and the retention time was 2.1 min. The quantification and detection limits were 1.0 μM and 0.3 μM,

Table 1
Efficiency of selective oxidation of 4-MBA to PAA for experiments in e^-NETmix in terms of conversion, consumed specific charge, selectivity to PAA, yield to PAA, and current efficiency (CE) for a reaction time of 120 min (columns on the left in bold) *versus* 50 % 4-MBA conversion (columns on the right).

e^-NETmix												
j **(mA cm^{-2})**	***t*** **(min)**		**Conversion (%)**		**Consumed specific charge (Ah L^{-1})**		**Selectivity to PAA (%)**		**Yield to PAA (%)**		**CE (%)**	
0.3	**120**	89	**61**	50	**0.059±0.002**	0.044±0.001	**82±2**	82±4	**50±2**	41±2	**45±2**	57±4
0.5	**120**	46	**84**	50	**0.099±0.002**	0.0379±0.0008	**80±4**	81±6	**67±4**	41±3	**36.2±0.8**	58±2
0.8	**120**	25	**96**	50	**0.158±0.002**	0.0329±0.0004	**82±1**	82±2	**79±2**	41±1	**26.8±0.4**	74±2
1.0	**120**	24	**97**	50	**0.198±0.002**	0.0394±0.0004	**74±3**	75±4	**72±3**	37±2	**19.4±0.3**	58±1
1.5	**120**	22	**98**	50	**0.297±0.002**	0.0552±0.0004	**74±2**	78.0±0.9	**72±2**	39±1	**13.0±0.2**	39±1
2.0	**120**	22	**98**	50	**0.396±0.002**	0.0715±0.0004	**65±3**	73.8±0.9	**64±3**	36.9±0.5	**8.6±0.1**	30±1
3.0	**120**	22	**98**	50	**0.594±0.002**	0.1069±0.0004	**47±3**	54±1	**46±3**	27±1	**4.2±0.1**	14.7±0.3
Re												
100	**120**	30	**94**	50	**0.158±0.002**	0.0398±0.0005	**85±4**	85±4	**80±4**	43±2	**27.1±0.4**	65±1
190	**120**	24	**97**	50	**0.158±0.002**	0.0316±0.0004	**82±1**	84±1	**79±2**	42±1	**26.9±0.4**	82±2
375	**120**	23	**97**	50	**0.158±0.002**	0.0305±0.0004	**82±2**	82±2	**80±2**	41±1	**27.0±0.4**	80±2
500	**120**	24	**97**	50	**0.158±0.002**	0.0316±0.0004	**83±2**	83±2	**80±2**	41±1	**27.1±0.4**	77±2
625	**120**	26	**96**	50	**0.158±0.002**	0.0339±0.0004	**83±1**	84±1	**80±2**	42±1	**27.0±0.4**	76±2
1000	**120**	26	**96**	50	**0.158±0.002**	0.0339±0.0004	**83±3**	83±3	**80±3**	42±1	**27.1±0.4**	74±2
1250	**120**	24	**97**	50	**0.158±0.002**	0.0316±0.0004	**82±1**	82±1	**80±2**	41±1	**27.1±0.4**	78±2
1750	**120**	25	**96**	50	**0.158±0.002**	0.0329±0.0004	**82±2**	82±2	**79±2**	41±1	**26.8±0.4**	74±2
$[Na_2SO_4]$ (mM)												
0	**120**	39	**88**	50	**0.158±0.002**	0.0514±0.0004	**80±2**	80±2	**70±3**	40±1	**23.7±0.4**	41.1±0.9
0.1	**120**	32	**92**	50	**0.158±0.002**	0.0428±0.0004	**80±1**	81.0±0.6	**74±2**	41±1	**25.0±0.4**	55±1
1	**120**	25	**97**	50	**0.158±0.002**	0.0327±0.0004	**80±2**	81±2	**77±2**	40±1	**26.1±0.4**	65±1
5	**120**	23	**97**	50	**0.158±0.002**	0.0308±0.0004	**80±2**	80.4±0.1	**78±2**	40±1	**26.4±0.4**	69±2
10	**120**	25	**96**	50	**0.158±0.002**	0.0332±0.0004	**82±1**	82±1	**79±1**	41±1	**26.8±0.4**	66±1
30	**120**	24	**97**	50	**0.158±0.002**	0.0316±0.0004	**82±2**	82±3	**79±2**	41±2	**26.9±0.4**	68±1
50	**120**	25	**96**	50	**0.158±0.002**	0.0329±0.0004	**82±2**	82±2	**79±2**	41±1	**26.8±0.4**	74±2
100	**120**	26	**96**	50	**0.158±0.002**	0.0339±0.0004	**82±2**	82±2	**79±2**	41±1	**26.7±0.4**	73±2
$[4\text{-MBA}]_0$ (mM)												
0.25	**120**	14	**100**	50	**0.158±0.002**	0.0191±0.0002	**77±1**	79.1±0.7	**77±1**	40±1	**6.5±0.2**	26.2±0.4
0.50	**120**	16	**99**	50	**0.158±0.002**	0.0217±0.0003	**82±2**	82±2	**81±3**	41±1	**13.8±0.3**	49.4±0.7
1.0	**120**	25	**96**	50	**0.158±0.002**	0.0329±0.0004	**82±2**	82±2	**79±2**	41±1	**26.8±0.4**	74±2
2.0	**120**	47	**83**	50	**0.158±0.002**	0.0627±0.0008	**91±3**	91±4	**76±3**	46±2	**51.1±0.7**	77±1
3.0	**120**	72	**68**	50	**0.158±0.002**	0.095±0.001	**89±3**	88±3	**61±3**	44±2	**61.8±0.8**	79±1

Table 2
Efficiency of selective oxidation of 4-MBA to PAA for experiments in e^-Cell in terms of conversion, consumed specific charge, selectivity to PAA, yield to PAA, and current efficiency (CE) for a reaction time of 120 min (columns on the left in bold) *versus* 50 % 4-MBA conversion (columns on the right).

e^-Cell											
j **(mA cm^{-2})**	***t*** **(min)**		**Conversion (%)**		**Consumed specific charge (Ah L^{-1})**		**Selectivity to PAA (%)**		**Yield to PAA (%)**		**CE (%)**	
0.3	**120**	99	**57**	50	**0.06±0.01**	0.049±0.008	**76±4**	78±3	**43±3**	39±7	**39±3**	51±8
0.5	**120**	51	**80**	50	**0.10±0.01**	0.042±0.004	**79±5**	80±6	**64±4**	40±5	**34±2**	58±6
0.8	**120**	39	**88**	50	**0.16±0.01**	0.051±0.003	**71±2**	71±2	**62±2**	35±2	**21±1**	42±3
1.0	**120**	36	**90**	50	**0.20±0.01**	0.060±0.003	**57±2**	57±1	**51±2**	28±1	**13.8±0.9**	29±1
1.5	**120**	35	**91**	50	**0.30±0.01**	0.087±0.003	**37±4**	42±2	**34±4**	21±1	**6.0±0.4**	13.2±0.6
2.0	**120**	38	**89**	50	**0.40±0.01**	0.126±0.003	**20±5**	26±6	**18±4**	13±3	**2.4±0.2**	6.1±0.3
3.0	**120**	37	**90**	50	**0.59±0.01**	0.182±0.003	**10±5**	15±1	**9±4**	7±1	**0.8±0.1**	2.3±0.2
Re												
100	**120**	124	**50**	50	**0.16±0.01**	0.16±0.01	**20±5**	22±5	**10±2**	11±2	**3.4±0.3**	3.6±0.3
190	**120**	81	**64**	50	**0.16±0.01**	0.106±0.007	**23±2**	24.0±0.5	**15±1**	12±1	**5.0±0.4**	6.1±0.5
375	**120**	77	**66**	50	**0.16±0.01**	0.102±0.006	**42±5**	41±5	**28±3**	21±3	**9.4±0.6**	10.8±0.8
500	**120**	71	**69**	50	**0.16±0.01**	0.093±0.006	**72±5**	72±5	**50±3**	36±3	**17±1**	25±2
625	**120**	75	**67**	50	**0.16±0.01**	0.098±0.006	**69±6**	69±4	**46±4**	35±3	**16±1**	23±1
1000	**120**	60	**75**	50	**0.16±0.01**	0.080±0.005	**70±6**	69±6	**52±5**	34±4	**18±1**	26±2
1250	**120**	41	**87**	50	**0.16±0.01**	0.054±0.003	**70±3**	70±2	**61±3**	35±2	**21±1**	36±2
1750	**120**	39	**88**	50	**0.16±0.01**	0.051±0.003	**71±2**	71±2	**62±2**	35±2	**21±1**	42±3
[Na_2SO_4] (mM)												
0	**120**	52	**80**	50	**0.16±0.01**	0.069±0.004	**66±6**	66±7	**52±5**	33±4	**18±1**	28±2
0.1	**120**	54	**79**	50	**0.16±0.01**	0.071±0.004	**70±5**	70±2	**55±4**	35±2	**19±1**	27±2
1	**120**	49	**82**	50	**0.16±0.01**	0.065±0.004	**72±3**	72±3	**59±3**	36±3	**20±1**	32±2
5	**120**	46	**83**	50	**0.16±0.01**	0.061±0.004	**71±2**	71±2	**59±2**	36±2	**20±1**	31±2
10	**120**	44	**85**	50	**0.16±0.01**	0.058±0.004	**67±3**	67.0±0.9	**57±3**	34±2	**19±1**	33±2
30	**120**	37	**90**	50	**0.16±0.01**	0.049±0.003	**67±3**	67±6	**60±3**	34±4	**20±1**	42±3
50	**120**	39	**88**	50	**0.16±0.01**	0.051±0.003	**71±2**	71±2	**62±2**	35±2	**21±1**	42±3
100	**120**	39	**88**	50	**0.16±0.01**	0.051±0.003	**71±4**	71±8	**62±4**	35±4	**21±1**	42±3
[4-MBA]$_0$ (mM)												
0.25	**120**	28	**95**	50	**0.16±0.01**	0.038±0.002	**52±8**	57±9	**49±8**	29±5	**4.2±0.4**	10.7±0.7
0.50	**120**	28	**95**	50	**0.16±0.01**	0.037±0.002	**60±5**	63±5	**57±5**	32±3	**9.6±0.6**	24±2
1.0	**120**	39	**88**	50	**0.16±0.01**	0.051±0.003	**71±2**	71±2	**62±2**	35±2	**21±1**	42±3
2.0	**120**	53	**79**	50	**0.16±0.01**	0.070±0.004	**75±4**	75±4	**59±3**	38±3	**40±3**	63±4
3.0	**120**	80	**65**	50	**0.16±0.01**	0.106±0.007	**92±4**	91±3	**59±3**	45±3	**60±4**	80±5

respectively. The methods were validated through the determination of linearity (R^2) and the limits of detection (LOD) and quantification (LOQ).

DOC was quantified by the difference between total dissolved carbon (TDC) and dissolved inorganic carbon (DIC): DOC = TDC – DIC. TDC was determined by catalytic combustion at 680 °C, and DIC was determined by acidification, both in a TC-TOC-TN analyzer with ASI-V autosampler (Shimadzu, model TOC-V_{CSN}) equipped with a nondispersive infrared (NDIR) detector.

LC-QTOF-MS/MS analysis and workflow followed in the initial identification of by-products is described in the Supplementary Material file.

Prior to HPLC, DOC, and LC-QTOF-MS/MS analysis, samples were filtered through 0.45 μm Nylon filters from Whatman.

Temperature and pH were measured by a multiparameter meter (HANNA, model edge® HI2020).

Total oxidants were determined using iodometric titration by adapting the procedure reported in Kolthoff and Carr [37]. In sum, (i) 10 mL of diluted sample were mixed with potassium iodide (KI) in excess and vigorously shaken and left to stand for 15 min, (ii) a volume of 5 mL of sulfuric acid (H_2SO_4) 5 % (v/v) was added to the mixture and shaken, and (iii) sodium thiosulfate ($Na_2S_2O_3$) 0.01 M was used to titrate the mixture under agitation until a change in color from yellowish to transparent-white was observed. The volume of $Na_2S_2O_3$ was registered to calculate the content of oxidants.

3. Results and discussion

3.1. Mechanism of 4-MBA oxidation on the FTO anode

First, the mechanism of 4-MBA oxidation on the bare FTO anode was electrochemically assessed by CV measurements. Fig. 2 shows that an aqueous solution of 100 mM Na_2SO_4 did not present any oxidation peak

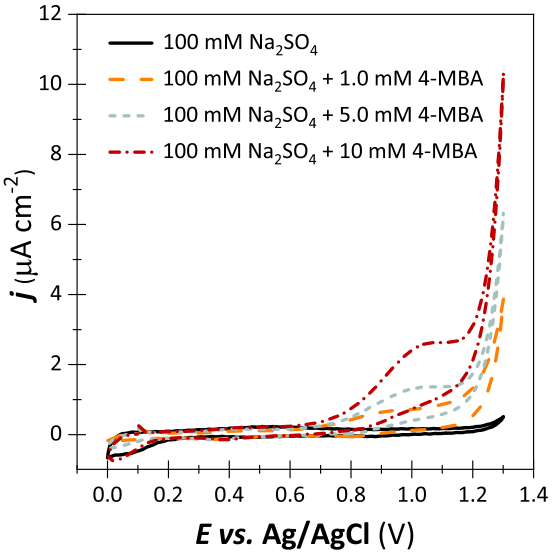

Fig. 2. CV curves for the bare FTO anode in a 100 mM Na_2SO_4 aqueous solution before and after adding different 4-MBA contents (T = 25±1 °C, scan rate of 10 mV s^{-1}).

until water oxidation onset at 1.25 V *vs.* Ag/AgCl. In contrast, the supporting electrolyte solution in the presence of 1.0 mM 4-MBA depicted a clear oxidation peak at around 1.0 V *vs.* Ag/AgCl that overlapped with the water oxidation onset at 1.2 V *vs.* Ag/AgCl. To associate the oxidation peak with the 4-MBA oxidation, increasing concentrations of 4-MBA up to 10 mM were applied. It can be observed that the *j* peak at 1.0 V *vs.* Ag/AgCl showed increasing values of 0.2 μA cm^{-2}, 0.7 μA cm^{-2}, 1.3 μA cm^{-2}, and 2.4 μA cm^{-2} at 0 mM, 1.0 mM, 5.0 mM, and 10 mM of 4-

MBA, respectively. A linear relation ($R^2 = 0.966$) between the j at 1.0 V *vs.* Ag/AgCl and the 4-MBA concentration can be obtained (Figure SM-2). These results suggest that the 4-MBA underwent direct charge transfer oxidation at the bare FTO anode.

The role of ROS in the 4-MBA oxidation was also assessed. ROS can be electrochemically generated from the oxidation of water and ions on the anode surface and contribute to the indirect oxidation of organics. Water oxidation mainly leads to the formation of physisorbed hydroxyl radicals ($^{\bullet}$OH) via Eq. (12) [3]. Oxidation of ions can promote the generation of distinct ROS, depending on the ions' nature. In the current work, the ions in the solution are sodium (Na^+) and sulfate (SO_4^{2-}), resulting from the supporting electrolyte (Na_2SO_4). While no ROS are typically formed from Na^+, SO_4^{2-} can provide the generation of persulfate ($S_2O_8^{2-}$) directly from SO_4^{2-} oxidation via Eq. (13) [1] and of sulfate radicals ($SO_4^{\bullet-}$) from various mechanisms, such as oxidation of SO_4^{2-} at the anode surface via Eq. (14) [38], reaction of $S_2O_8^{2-}$ with $^{\bullet}$OH or an organic (R) via Eqs. (15) or (16) [39], and reduction of $S_2O_8^{2-}$ via Eq. (17) [40]. The possible contribution of $^{\bullet}$OH, $SO_4^{\bullet-}$, and $S_2O_8^{2-}$ to the 4-MBA oxidation was evaluated.

$$H_2O \rightarrow {}^{\bullet}OH + H^+ + e^- \quad (12)$$

$$2SO_4^{2-} \rightarrow S_2O_8^{2-} + 2e^- \quad (13)$$

$$SO_4^{2-} \rightarrow SO_4^{\bullet-} + e^- \quad (14)$$

$$S_2O_8^{2-} + {}^{\bullet}OH \rightarrow HSO_4^- + SO_4^{\bullet-} + 1/2O_2 \quad (15)$$

$$S_2O_8^{2-} + R \rightarrow 2SO_4^{\bullet-} + R^{\bullet} \quad (16)$$

$$S_2O_8^{2-} + e^- \rightarrow SO_4^{2-} + SO_4^{\bullet-} \quad (17)$$

Regarding $^{\bullet}$OH and $SO_4^{\bullet-}$, their role was determined by carrying out standard 4-MBA oxidation reactions in e^-NETmix (conditions: j = 0.8 mA cm^{-2}, Re = 1750, $[Na_2SO_4]$ = 50 mM, $[4\text{-MBA}]_0$ = 1.0 mM, T = 25±1 °C, pH = 7.0±0.2), both in the absence and presence of $^{\bullet}$OH and $SO_4^{\bullet-}$ scavengers. Tert-butyl alcohol (TBA) and N,N'-dimethylthiourea (DMTU) were used as $^{\bullet}$OH scavengers, while methanol (MeOH) was used as $SO_4^{\bullet-}$ scavenger. Contents of 10–100 mM TBA, 10–25 mM DMTU, and 10–100 mM MeOH were employed. There was no change in the 4-MBA decay or PAA formation in the presence of the scavengers (data not shown), which excludes the contribution of $^{\bullet}$OH and $SO_4^{\bullet-}$ to the 4-MBA oxidation.

The involvement of $S_2O_8^{2-}$ in the 4-MBA oxidation was indirectly inferred by determining the concentration of total oxidants in the solution (using iodometric titration) during a standard 4-MBA oxidation reaction in e^-NETmix. The content of total oxidants was null during the reaction according to the LOD of the analytical method (data not shown). Thus, it is unlikely that the $S_2O_8^{2-}$ may have participated in the 4-MBA oxidation. Note that the content of $^{\bullet}$OH and $SO_4^{\bullet-}$ cannot be deduced by iodometric titration due to the short lifetimes of these radicals in water in the order of few ns [41] or dozens of μs [42], respectively, and due to the restriction of their action to the anode vicinity.

The results mentioned above suggest that ROS did not contribute to the 4-MBA oxidation and, therefore, the 4-MBA may have been exclusively oxidized by direct charge transfer oxidation at the FTO anode. This is an expected outcome regarding the low applied j (0.8 mA cm^{-2}) and consequent low E_{cell} (~3.0 V), which do not favor the generation of the scrutinized ROS [1].

Based on these findings, one can suggest a reaction pathway for the 4-MBA selective oxidation to PAA: the FTO anode captures an electron from the 4-MBA, giving rise to the corresponding cation radical, which suffers further oxidation, evolving to PAA and other possible by-products. In total, two electrons are exchanged per molecule of PAA formed. Fig. 3 illustrates the 4-MBA oxidation reactions.

3.2. By-products of 4-MBA oxidation on the FTO anode

The 4-MBA oxidation leads to the generation of PAA, the target product, but other products can be formed since a selectivity of 100 % to a given product is challenging. A LC-QTOF-MS/MS analysis investigated the formation of by-products in a first approach. Samples from standard 4-MBA oxidation reactions (conditions: $[Na_2SO_4]$ = 50 mM, $[4\text{-MBA}]_0$ = 1.0 mM, T = 25±1 °C, pH = 7.0±0.2) were analyzed, either taking place in the e^-NETmix reactor (Re = 1750) under constant current conditions (j = 0.8 mA cm^{-2}) or in the undivided batch cell under potentiostatic conditions (E = 1.0 V *vs.* Ag/AgCl). This determination revealed the presence of a single product apart from PAA: the 4-methoxybenzoic acid (4-MBZA). The obtained MS/MS spectra for PAA and 4-MBZA are given in Figures SM-3 and SM-4, respectively. Afterward, the 4-MBZA, PAA, and CO_2 were quantified by HPLC or DOC analysis for a standard 4-MBA oxidation reaction in the e^-NETmix device. The carbon balance of this reaction for 50 % 4-MBA conversion revealed that, in addition to 50 % of C in the 4-MBA form, 41 % of C was in the PAA form (selectivity to PAA of 82 %), 7.7 % of C was in CO_2 form, and the remaining 1.3 % C was in the 4-MBZA form (Figure SM-5). An extra trial, in which 1.0 mM PAA was the feeding solution, proved that the 4-MBZA compound derived from PAA partial oxidation. Furthermore, the 4-MBA oxidation to PAA proved to be irreversible. Loddo et al. [43], Palmisano et al. [24], and Yurdakal et al. [25] reported that CO_2 was the main oxidation product, apart from PAA, in photocatalytic experiments starting from 4-MBA, and that there were traces of 4-MBZA, in agreement with the outcomes achieved here.

3.3. Selective electrochemical oxidation of 4-MBA to PAA

The 4-MBA selective electrooxidation to PAA was assessed for different j (from 0.3 mA cm^{-2} to 3.0 mA cm^{-2}), hydrodynamic conditions in terms of Re (from 100 to 1750), supporting electrolyte (Na_2SO_4) contents (from 0 mM to 100 mM), and substrate 4-MBA initial contents (from 0.25 mM to 3.0 mM). The impact of a specific operational

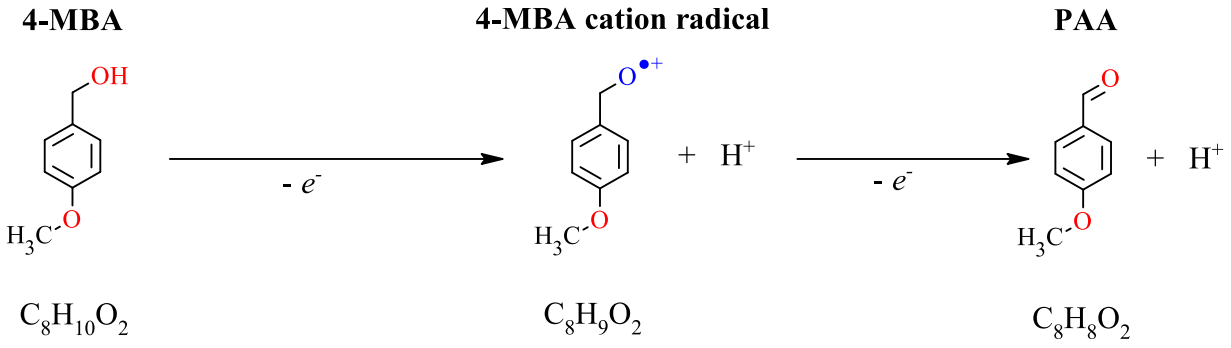

Fig. 3. Direct electrooxidation pathway of 4-MBA to PAA.

parameter on the selective oxidation of 4-MBA to PAA was evaluated while keeping the other operational parameters constant. In this regard, (i) while varying the *j*, Na_2SO_4 content and 4-MBA initial content, the *Re* was fixed at 1750, which is the maximum *Re* permitted in the current electrochemical system employing the e^-Cell technology, (ii) while changing the *Re*, *j* and 4-MBA initial content, the Na_2SO_4 content was kept at 50 mM, which typically ensures an excess of supporting electrolyte and protects the oxidation reactions from migratory effects [44, 45], (iii) while varying the *Re*, *j* and Na_2SO_4 content, the 4-MBA initial content was fixed at 1.0 mM since it is a value within the range of the most widely employed 4-MBA initial contents [21, 23–25], and (iv) while varying the *Re*, Na_2SO_4 content and 4-MBA initial content, the *j* was fixed at 0.8 mA cm^{-2} since this *j* value provided maximum PAA production rates for a *Re* of 1750 and a 4-MBA initial content of 1.0 mM in e^-NETmix and e^-Cell (see Section 3.3.1).

3.3.1. *Influence of current density*

The increase of *j* promoted larger $r_{0,4\text{-MBA}}$ values for j <0.8 mA cm^{-2} and minimal changes in the $r_{0,4\text{-MBA}}$ values for $j \geq 0.8$ mA cm^{-2}, both in e^-NETmix and e^-Cell (Figs. 4a and 4c and Tables SM-1 and SM-2). The positive effect of *j* on the $r_{0,4\text{-MBA}}$ up to 0.8 mA cm^{-2} can be attributed to the occurrence of 4-MBA direct charge transfer oxidation to a greater degree. This indicates that the 4-MBA oxidation was charge transfer controlled for j <0.8 mA cm^{-2}. Upon applying $j \geq 0.8$ mA cm^{-2}, the 4-MBA oxidation may have no longer been controlled by charge transfer. The two reactors differed in the maximum obtained $r_{0,4\text{-MBA}}$. This parameter was $(30\pm3)\times10^{-3}$ mM min^{-1} in e^-NETmix and $(19\pm1)\times10^{-3}$ mM min^{-1} in e^-Cell ((1.6±0.2)-fold greater in e^-NETmix). Since the other parameters affecting the $r_{0,4\text{-MBA}}$ were similar in both reactors, this outcome can be attributed to mass transfer limitations in the e^-Cell reactor due to its poorer mass transfer performance. The k_mA and k_m values were ~52-fold and ~7.1-fold smaller in e^-Cell compared to e^-NETmix for a *Re* of 1750 [9].

The selectivity to PAA is directly related to the specific pathway of 4-MBA oxidation and PAA further oxidation to other products, namely CO_2 and 4-MBZA. In both reactors, the selectivity to PAA had a similar maximum value at low *j*, and the application of larger *j* negatively impacted this parameter (Figs. 4a and 4c). The registered maximum selectivity was 79±8 % for both reactors. The detrimental effect of *j* on the selectivity can be attributed to PAA's electrochemical instability and its overoxidation at a higher degree as increasing currents are supplied. The two reactors differed in the *j* value at which this negative effect is initiated and in the extent of this effect. While the selectively was negatively impacted for j >2.0 mA cm^{-2} in e^-NETmix, this adverse impact started occurring for j >0.5 mA cm^{-2} in e^-Cell. Furthermore, the selectivity decreased by (1.5±0.2)-fold upon the increase of *j* from

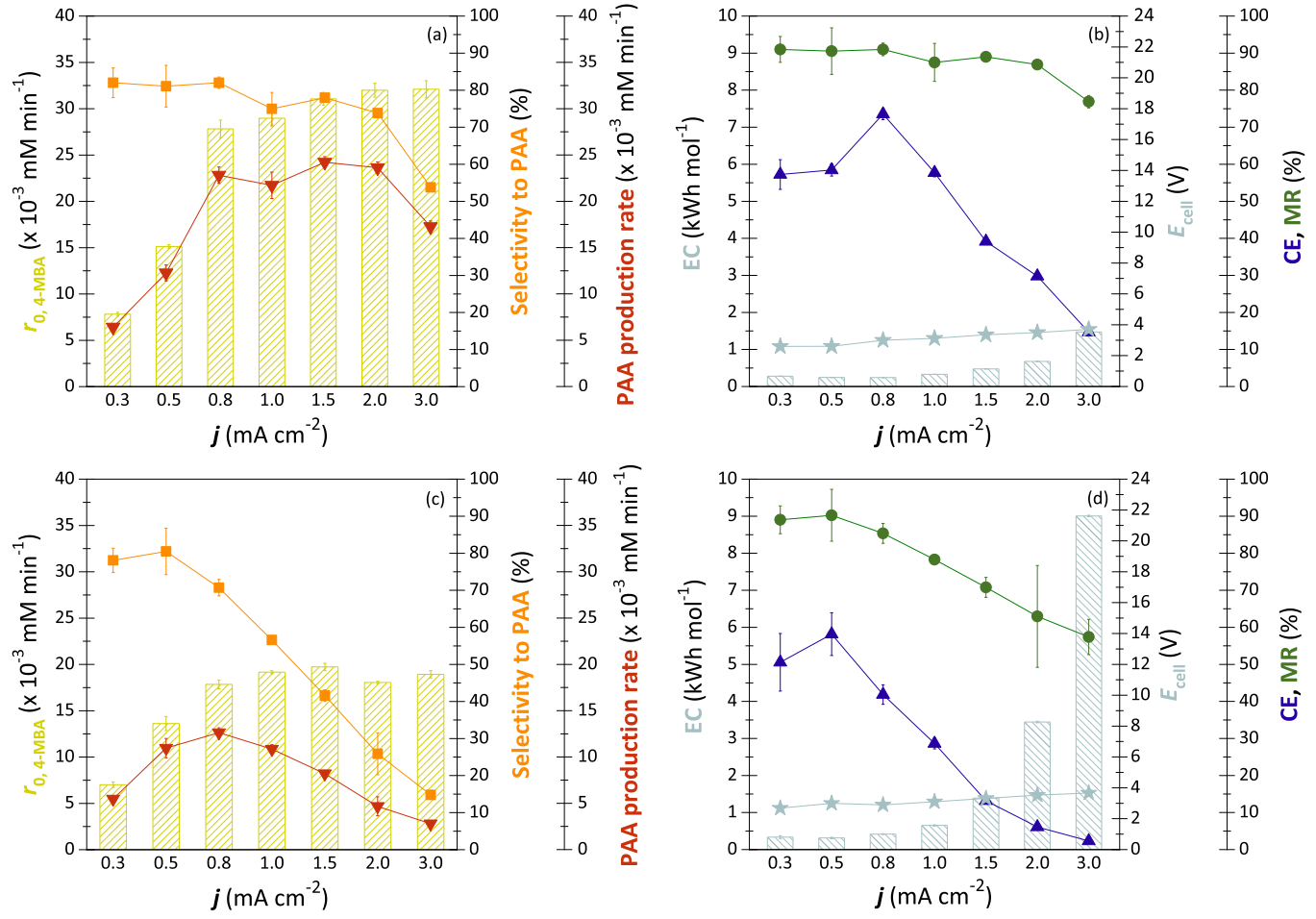

Fig. 4. Efficiency of selective oxidation of 4-MBA to PAA as a function of current density in e^-NETmix (a, b) and e^-Cell (c, d). Efficiency in terms of 4-MBA initial oxidation rate ($r_{0,4\text{-MBA}}$) (▨), selectivity to PAA (■), and PAA production rate (▼) (a, c); and energy consumption for electrical current supply (EC) (▨), average cell potential (E_{cell}) (★), current efficiency (CE) (▲), and material recovery (MR) (●) (b, d). Values for 50 % 4-MBA conversion. Conditions: *Re* = 1750, $[Na_2SO_4]$ = 50 mM, $[4\text{-MBA}]_0$ = 1.0 mM, *T* = 25±1 ºC, pH = 7.0±0.2. Error bars are representative of deviations from duplicate trials.

2.0 mA cm^{-2} to 3.0 mA cm^{-2} in e^{-}NETmix, whereas there was an abrupt decrease in the selectivity of (5.4±0.7)-fold in e^{-}Cell for a rise in the j from 0.5 mA cm^{-2} to 3.0 mA cm^{-2}. Therefore, a lower effect of j on the selectivity in the e^{-}NETmix reactor is evident, which can be ascribed to the enhanced mass transfer in this reactor. In the presence of more intense mass transfer phenomena, the PAA can be removed faster from the active sites of the FTO anode, which can hinder its overoxidation. One can claim that e^{-}NETmix protected the PAA from overoxidation.

The effect of j on the $r_{0,4\text{-MBA}}$ and selectivity to PAA simultaneously contributed to a maximum PAA production rate of (23±4)×10^{-3} mM min^{-1} for a wide j range of 0.8–2.0 mA cm^{-2} in e^{-}NETmix. This contrasted to a maximum PAA production rate of (12.6±0.5)×10^{-3} mM min^{-1} in e^{-}Cell ((1.8±0.2)-fold smaller) for a single j value of 0.8 mA cm^{-2} (Figs. 4a and 4c).

The EC values were (1.2±0.1)-fold smaller for j <0.8 mA cm^{-2} in the e^{-}NETmix reactor compared to the e^{-}Cell reactor (Figs. 4b and 4d) due to the slightly larger magnitude of $r_{0,4\text{-MBA}}$ in the former reactor. For j in the range 0.8–3.0 mA cm^{-2}, the disparity between the two reactors in terms of EC became notably pronounced and intensified with increasing j. This finding can be ascribed to the dramatic decrease in selectivity to PAA observed in the e^{-}Cell reactor for j ≥0.8 mA cm^{-2}.

The maximum MR value was 89±8 % in both reactors (Figs. 4b and 4d) due to the similar maximum selectivity to PAA. Note that the MR exhibits identical behavior as the selectivity to PAA because of its calculation for a fixed 4-MBA conversion of 50 %. The same trend is observed for the yield to PAA, as illustrated by the values presented in Table 1 and Table 2 (values for 50 % conversion). The maximum CE was similar in e^{-}NETmix and e^{-}Cell (74±2 % and 58±6 %, respectively) but was achieved for distinct j (Figs. 4b and 4d). The CE was maximum at 0.8 mA cm^{-2} in e^{-}NETmix and at a lower j of 0.5 mA cm^{-2} in e^{-}Cell because of the decrease in selectivity for j >0.5 mA cm^{-2} in the latter reactor. After reaching the maximum, the CE decreased as j increased in both reactors. This can be attributed to the boost of the rate of parasitic reactions, including the oxygen (O_2) evolution at the anode surface through water oxidation via Eq. (18) [1], and, when applicable, to the above-mentioned drop of selectivity.

$$^{\bullet}OH + H_2O \rightarrow O_2 + 3H^{+} + 3e^{-} \quad (18)$$

Table 1 and Table 2 present a summary of results obtained in e^{-}NETmix and e^{-}Cell, respectively, for 120 min of reaction, resulting in conversions ranging from >50–98 %. The key disparity observed at higher conversion levels in both reactors pertains to CE. As conversions increased, CE decreased, achieving values from 1.3±0.1 % to 3.5±0.1 % lower for j ranging from 0.3 mA cm^{-2} to 3.0 mA cm^{-2}. This CE decline can be attributed to the escalation of parasitic reactions at higher conversions. The highest CE was achieved at a j of 0.3 mA cm^{-2} in both

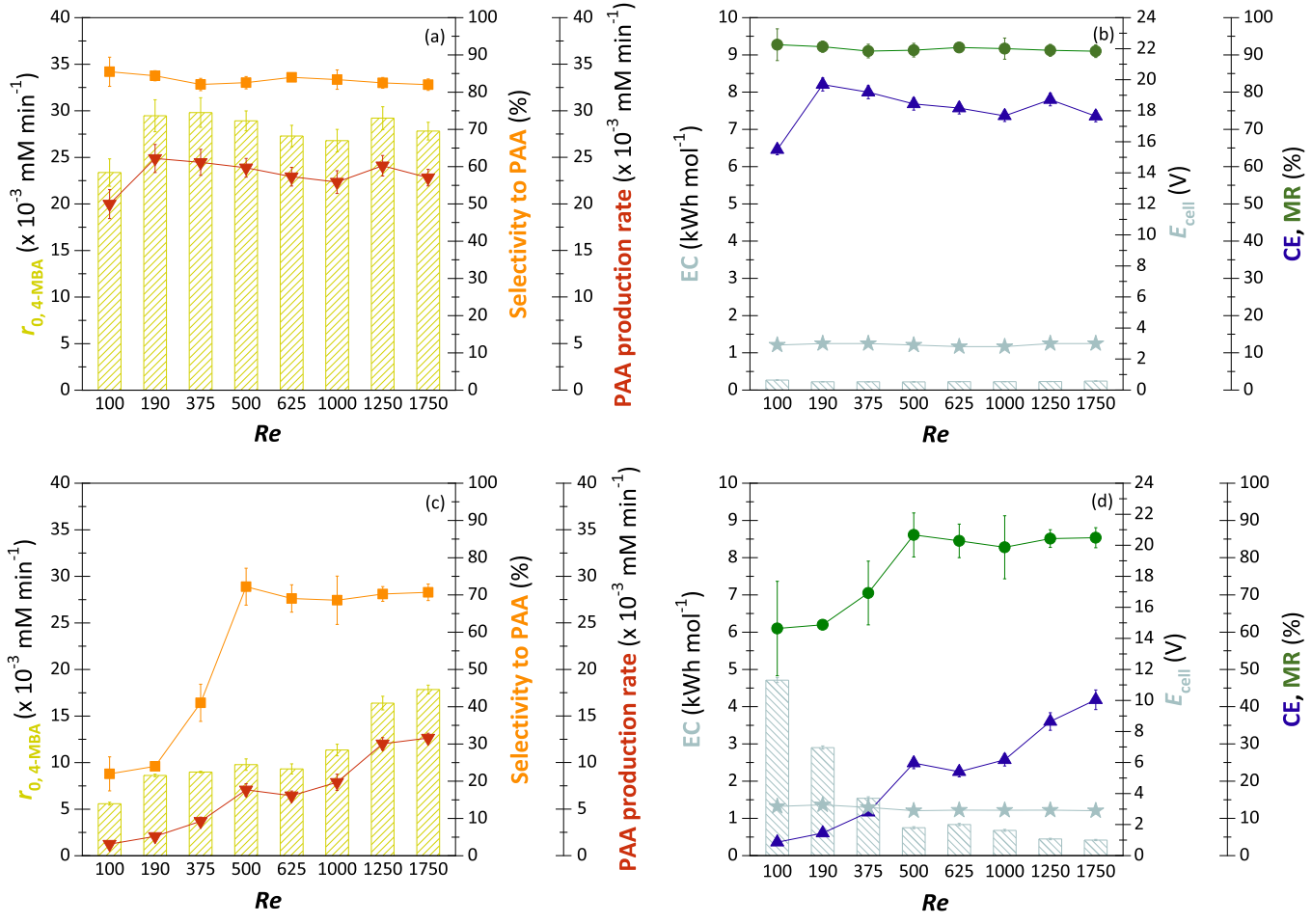

Fig. 5. Efficiency of 4-MBA selective oxidation to PAA as a function of hydrodynamics (Reynolds number – *Re*) in e^{-}NETmix (a, b) and e^{-}Cell (c, d). Efficiency in terms of 4-MBA initial oxidation rate ($r_{0,4\text{-MBA}}$) (▨), selectivity to PAA (▼), and PAA production rate (▼) (a, c); and energy consumption for electrical current supply (EC) (▨), average cell potential (E_{cell}) (★), current efficiency (CE) (▲), and material recovery (MR) (●) (b, d). Values for 50 % 4-MBA conversion. Conditions: j = 0.8 mA cm^{-2}, [Na_2SO_4] = 50 mM, [4-MBA]$_0$ = 1.0 mM, T = 25±1 °C, pH = 7.0±0.2. Error bars are representative of deviations from duplicate trials.

reactors, with values reaching 45±2 % and 39±9 % in e^-NETmix and e^-Cell, respectively. The yield to PAA increased as a consequence of the increase in conversion, achieving peak values of 79±2 % and 62±2 % in e^-NETmix and e^-Cell, respectively, at a j of 0.8 mA cm^{-2}, at which a consumed charge of ~0.16 Ah L^{-1} was obtained in both reactors.

3.3.2. Influence of hydrodynamics (Reynolds number)

In the e^-NETmix reactor, *Re* of 100–1750 translates to flow rates of 6.7–118.0 L h^{-1}, residence times of 3.98–0.22 s, and number of passes through the reactor of 904–16,364 within each 60-min interval. In e^-Cell, *Re* of 100–1750 correspond to flow rates of 4.3–75.5 L h^{-1}, residence times of 3.35–0.19 s, and number of passes through the reactor of 1075–18,947 within each 60-min interval. Residence times and number of passes exhibit remarkable similarity across both reactors.

The increase of *Re* from 100 to 190 in the e^-NETmix reactor promoted a slight growth in the $r_{0,4\text{-MBA}}$ value ((1.3±0.1)-fold), and minimal variations were achieved for higher *Re* (Fig. 5a and Table SM-1). A maximum $r_{0,4\text{-MBA}}$ value of (28±3)×10^{-3} mM min^{-1} was achieved for 190≤*Re*≤1750. In the e^-Cell technology, the effect of *Re* was very distinct. Increasing $r_{0,4\text{-MBA}}$ values were attained for rising *Re* for all the tested range (100≤*Re*≤1750) (Fig. 5c and Table SM-2). Moreover, the $r_{0,4\text{-MBA}}$ values were (4.3±0.3)-fold to (1.5±0.1)-fold inferior to those in e^-NETmix. The largest *Re* (1750) could not provide the maximum $r_{0,4\text{-MBA}}$ value achieved in the e^-NETmix device, indicating that there was a lot of room for enhancing the $r_{0,4\text{-MBA}}$ in e^-Cell. These results suggest that the 4-MBA oxidation in the e^-NETmix reactor was slightly mass transfer limited for a *Re* of 100, and no mass transfer limitations occurred for *Re* ≥190. On the other hand, the 4-MBA oxidation in the e^-Cell reactor may have been mass transfer controlled for all *Re*.

Regarding the selectivity to PAA, *Re* had a null effect on this parameter in e^-NETmix (Fig. 5a). By contrast, increasing selectivity values were observed up to a *Re* of 500 in e^-Cell, followed by similar values onwards (Fig. 5c). The lower selectivity in e^-Cell for *Re* <500 can be associated with the PAA overoxidation due to mass transfer limitations. It was necessary to reach a k_mA of (4.7±0.5)×10^{-3} s^{-1}, i.e., the k_mA for *Re* of 500 in e^-Cell [9], to maximize the selectivity. The k_mA values in e^-NETmix were always larger than (1.29±0.03)×10^{-1} s^{-1} [9], which can explain the achievement of a maximum selectivity regardless of the *Re* in this reactor. The magnitude of the maximum selectivity in both reactors was also distinct. While the selectivity had a maximum value of 83±6 % in e^-NETmix (for the entire *Re* range), the maximum selectivity was 70±8 % in e^-Cell (for *Re* ≥500). A slightly smaller selectivity was expected in the e^-Cell reactor since applying a j of 0.8 mA cm^{-2} leads to a slightly prejudicial effect on this parameter, according to Section 3.3.1.

The PAA production rate was maximum for a wide *Re* range of 190–1750 (flow rates of 12.8 L h^{-1} to 118.1 L h^{-1}) and equal to (23±5)×10^{-3} mM min^{-1} in e^-NETmix (Fig. 5a). Conversely, the PAA production rate was ever-increasing in e^-Cell, reaching a maximum of (12.6±0.5)×10^{-3} mM min^{-1} ((1.8±0.4))-fold smaller compared to the e^-NETmix set-up) for a *Re* of 1750 (flow rate of 76.5 L h^{-1}) (Fig. 5c). The CE behavior was similar, reaching a maximum of 77±7 % in the e^-NETmix reactor for *Re* ≥190 (Fig. 5b) and a value (1.8±0.2)-fold lower in e^-Cell for a *Re* of 1750 (Fig. 5d).

The EC consistently exhibited higher values in e^-Cell compared to the e^-NETmix reactor (Figs. 5b and 5d) due to the lower $r_{0,4\text{-MBA}}$ values in the former reactor. For *Re* 100–375, this difference became much more pronounced owing to the decreased selectivity to PAA in e^-NETmix, resulting in a (12.9±0.2)-fold larger value in the e^-Cell reactor for *Re* 100. The two reactors' slightly different maximum selectivity values led to maximum MR values of 92±5 % and 85±6 % in e^-NETmix and e^-Cell reactors, respectively (Figs. 5b and 5d).

From the data presented in Table 1 and Table 2, it becomes evident that higher conversions led to lower CE and higher yield to PAA. At 120 min of reaction and a consumed charge of ~0.16 Ah L^{-1}, the CE achieved values of 26.8±0.4 % and 21±1 % in e^-NETmix and e^-Cell, respectively, and the yield to PAA was 79±2 % and 62±2 %, respectively. No additional changes were observed at higher conversion levels.

Employing lower *Re* (flow rates) while maintaining maximum performance, as facilitated by e^-NETmix, can confer significant advantages due to, for example, (i) the reduction of the energy consumption for pumping the fluid, which is both environmentally beneficial and cost-effective, (ii) the minimization of the wear and tear of the electrodes and equipment, such as pumps, valves, and pipes, potentially extending their lifespan and reducing maintenance costs, (iii) the ease of handling and automating processes, and (iv) the reduced demands on equipment size and capacity, and consequent ease of scaling-up processes.

3.3.3. Effect of supporting electrolyte content

The operation without a supporting electrolyte, i.e., the so-called self-supported bulk electrolysis, was possible for both reactors. This can be attributed to the short distance between the electrodes, which enables the charge to still be transferred even in the absence of a supporting electrolyte. However, the application of distinct Na_2SO_4 contents highly affected the energy consumption for the supply of electrical power to the reactors, represented by the EC (Figs. 6b and 6d). The EC was (6.5±0.3)-fold and (3.6±0.1)-fold smaller in e^-NETmix compared to the e^-Cell reactor in the lack of supporting electrolyte and in the presence of a low Na_2SO_4 content of 0.1 mM, respectively. The very distinct EC values in both reactors for null or low Na_2SO_4 concentrations can be mainly attributed to the much larger E_{cell} registered in e^-Cell (Figs. 6b and 6d). For instance, an average E_{cell} as high as 16.2 V was obtained in e^-Cell in the absence of a supporting electrolyte, contrasting with a E_{cell} of 3.8 V in e^-NETmix under the same conditions. The higher E_{cell} in e^-Cell resulted from a higher ohmic resistance in this reactor mainly due to its wider interelectrode gap (3.8 mm in e^-Cell *versus* 0–1.5 mm in e^-NETmix). As the Na_2SO_4 content increased, the difference in the registered EC values in the two reactors became blurred due to the smaller ohmic resistances achieved for higher supporting electrolyte contents and, consequently, similar E_{cell}. For Na_2SO_4 contents ≥1 mM in e^-NETmix and ≥30 mM in e^-Cell, an average E_{cell} of 3.0 ±0.1 V was recorded in both reactors, and the EC values were (1.8±0.2)-fold smaller in the e^-NETmix device exclusively due to the smaller $r_{0,4\text{-MBA}}$ in this reactor, as discussed below.

The Na_2SO_4 content also impacted the $r_{0,4\text{-MBA}}$ values (Figs. 6a and 6c and Tables SM-1 and SM-2), although to a lower extent than for EC. The $r_{0,4\text{-MBA}}$ values were positively affected by the Na_2SO_4 content in both reactors up to a given Na_2SO_4 content from which the $r_{0,4\text{-MBA}}$ values became similar. The achievement of smaller $r_{0,4\text{-MBA}}$ values for lower Na_2SO_4 contents was likely due to the mass transfer of electroactive species by migration in the absence of a supporting electrolyte in excess. The transport of species by migration is usually complicated and known by disturbing the mass transfer properties by diffusion and/or convection so intensively that data interpretation becomes difficult or impossible [44]. Moreover, the supporting electrolyte content is inversely proportional to the thickness of the electrical double layer (EDL), and, thus, there is additional flow resistance under low electrolyte contents, ultimately changing the $r_{0,4\text{-MBA}}$ values via electrokinetic effects [46,47]. During the phase when the $r_{0,4\text{-MBA}}$ values ceased to depend on the Na_2SO_4 content, the Na_2SO_4 may have been available in excess. This may have eliminated the migratory effects, and, thus, the mass transfer may have occurred exclusively by diffusion and convection, and the EDL may have remained thin.

The two reactors differed in the Na_2SO_4 content for which $r_{0,4\text{-MBA}}$ stopped depending on the Na_2SO_4 content – 1 mM in e^-NETmix *versus* 30 mM in e^-Cell. This can be mainly associated with the enhanced mass transfer by convection and diffusion in this reactor. Because of that, the e^-NETmix reactor may have been more able to protect electroactive species from migratory effects. Furthermore, the $r_{0,4\text{-MBA}}$ values in e^-Cell were always smaller (by (1.34±0.06) to (2.0±0.1)-fold) irrespective of the supporting electrolyte content. The maximum $r_{0,4\text{-MBA}}$ value was (28±2)×10^{-3} mM min^{-1} in e^-NETmix (for 4-MBA initial

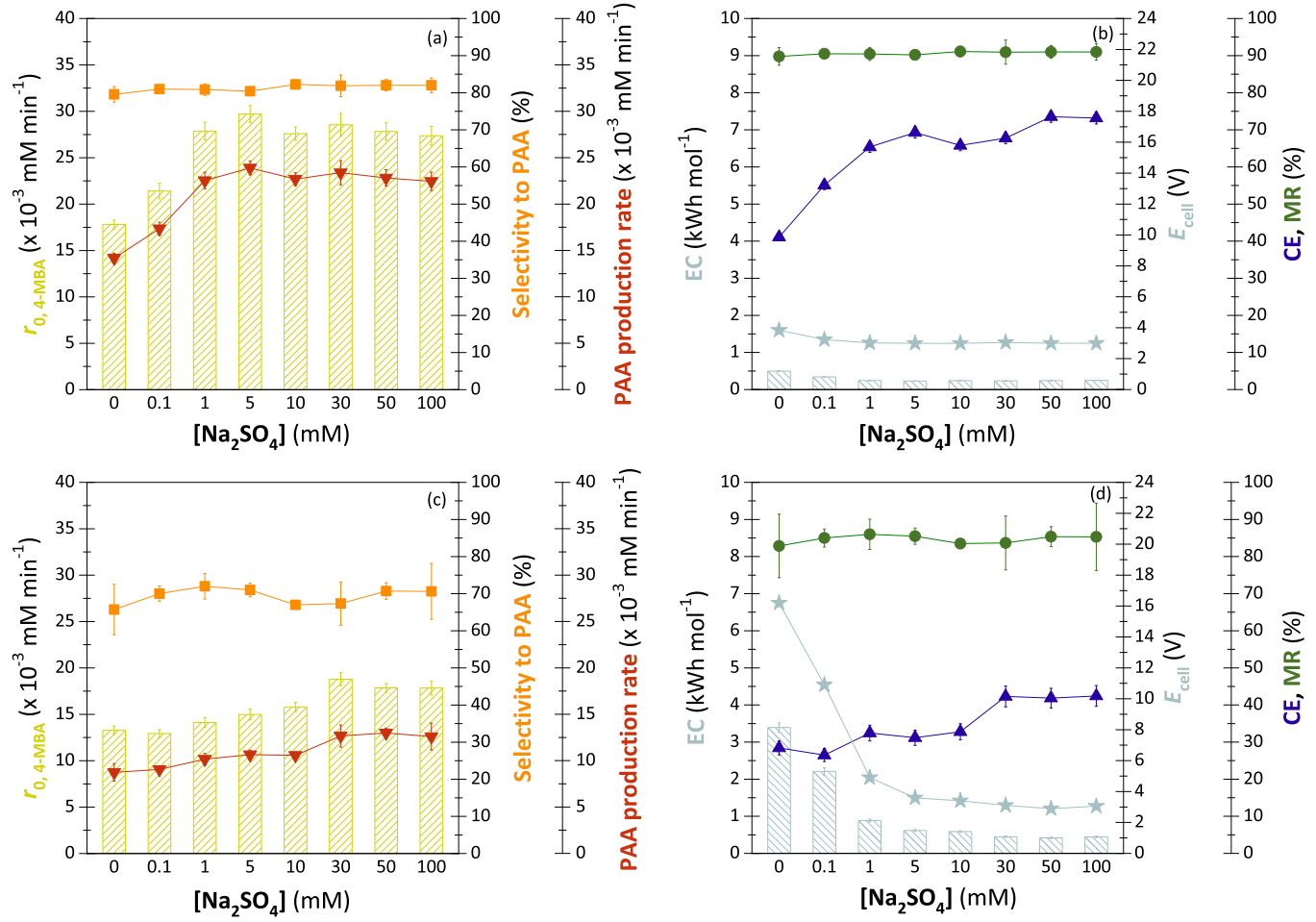

Fig. 6. Efficiency of selective oxidation of 4-MBA to PAA as a function of supporting electrolyte (Na_2SO_4) content in e^-NETmix (a, b) and e^-Cell (c, d). Efficiency in terms of 4-MBA initial oxidation rate ($r_{0,4\text{-MBA}}$) (▨), selectivity to PAA (■), and PAA production rate (▼) (a, c); and energy consumption for electrical current supply (EC) (▨), average cell potential (E_{cell}) (★), current efficiency (CE) (▲), and material recovery (MR) (●) (b, d). Values for 50 % 4-MBA conversion. Conditions: j = 0.8 mA cm^{-2}, Re = 1750, $[4\text{-MBA}]_0$ = 1.0 mM, T = 25±1 °C, pH = 7.0±0.2. Error bars are representative of deviations from duplicate trials.

contents ≥1 mM) and (18±1)×10^{-3} mM min^{-1} in e^-Cell (for 4-MBA initial contents ≥30 mM). The smaller $r_{0,4\text{-MBA}}$ values achieved in the e^-Cell reactor can be mainly related to the inability to maximize the 4-MBA oxidation in this reactor due to mass transfer limitations, even for a Re of 1750. This contrasts with the absence of constraints in the transport of the 4-MBA for Re ≥190 in e^-NETmix, as discussed in Section 3.3.2. It should also be mentioned that the ratio of supporting electrolyte concentration to electroactive species bulk concentration that allowed for a maximization of the $r_{0,4\text{-MBA}}$ was 1-fold in e^-NETmix and 30-fold in e^-Cell. The ratio in the e^-NETmix device was lower than the usually reported ratios, i.e., 10 to >100-fold [44,45], while the ratio in the e^-Cell set-up was within the commonly disclosed values. These outcomes highlight the improvement of mass transfer by convection and diffusion in this novel reactor.

The selectivity to PAA was not affected by the supporting electrolyte content in both reactors (Figs. 6a and 6c). Selectivity values of 81±2 % in e^-NETmix and 69±9 % in e^-Cell were achieved in the full range of Na_2SO_4 contents. These results suggest a null influence of the migratory effects and EDL thickness on transferring the generated PAA from the anode surface to the bulk solution. The slightly lower average selectivity attained in e^-Cell can be related to the application of a j of 0.8 mA cm^{-2}, which showed a slight adverse effect on the selectivity, as discussed in Section 3.3.1. The MR values, which had the same behavior as the selectivity to PAA, were 91±2 % and 85±10 % in e^-NETmix and e^-Cell, respectively, for the entire Na_2SO_4 content range (Figs. 6b and 6d).

As the selectivity remained constant for all the supporting electrolyte contents in both reactors, the PAA production rate had the same behavior as the $r_{0,4\text{-MBA}}$. In the e^-NETmix reactor, the PAA production rate was maximum and equal to (23±2)×10^{-3} mM min^{-1} for Na_2SO_4 contents ≥1 mM (Fig. 6a); in the e^-Cell reactor, the PAA production rate was maximum and equal to (13±1)×10^{-3} mM min^{-1} ((1.8±0.2)-fold lower) for Na_2SO_4 contents ≥30 mM (Fig. 6c). The CE also had the same behavior as the $r_{0,4\text{-MBA}}$, with a maximum of 69±6 % in e^-NETmix (Fig. 6b) and 42±3 % in e^-Cell (Fig. 6d).

The application of higher conversions promoted lower CE and higher yield to PAA, without any further discernible alterations (see Tables 1 and 2). This trend mirrors the observations made for j and Re.

Note that the generation of ROS from the SO_4^{2-} ions provided by the Na_2SO_4 was not detected (see Section 3.1). Consequently, there was no intensification of indirect oxidation mechanisms upon using higher Na_2SO_4 concentrations.

The use of low supporting electrolyte contents without loss of efficiency, as permitted in the e^-NETmix technology, can be very advantageous. For instance, it can contribute to (i) cost savings since supporting electrolytes can be expensive, (ii) the mitigation of the electrode fouling, thereby prolonging the lifespan of the electrodes, (iii)

the simplification of the scaling-up process as the challenges related to the handling of large volumes of electrolyte solutions are avoided, (iv) simpler purification procedures and higher product yields since high concentrations of electrolytes can complicate the separation and purification of the target products, and (v) the improvement of the selectivity when the supporting electrolyte leads to undesirable side reactions.

3.3.4. *Effect of substrate initial content*

The $r_{0,4\text{-MBA}}$ values increased for larger 4-MBA initial contents in both reactors up to a plateau characterized by similar $r_{0,4\text{-MBA}}$ values regardless of the 4-MBA initial content. This plateau was achieved for 4-MBA initial contents ≥1.0 mM in e^-NETmix and ≥2.0 mM in e^-Cell (Figs. 7a and 7c and Tables SM-1 and SM-2). The $r_{0,4\text{-MBA}}$ growth phase indicates that larger 4-MBA contents were made available at the FTO anode surface to interact with the free active sites and undergo direct oxidation when larger 4-MBA initial contents were present. Therefore, it can be claimed that the 4-MBA oxidation at the FTO anode was under mass transfer control for 4-MBA initial contents <1.0 mM in e^-NETmix and <2.0 mM in e^-Cell. In this growth phase, the $r_{0,4\text{-MBA}}$ values were (1.56±0.08) to (2.0±0.1)-fold lower in the e^-Cell device than in the e^-NETmix device. This can be ascribed to a lower mass transfer of the 4-MBA to the anode surface in the former reactor. In the plateau phase, the content of 4-MBA in solution may have been sufficiently high to saturate the FTO active sites, avoiding mass transfer limitations and equalizing the $r_{0,4\text{-MBA}}$ values in both reactors – (29±2)×10^{-3} mM min^{-1}. The need for double the 4-MBA initial content in the e^-Cell reactor compared to the e^-NETmix reactor to attain this phase (2.0 mM *versus* 1.0 mM) corroborates the poorer mass transport of the 4-MBA to the anode surface in e^-Cell.

Regarding selectivity to PAA, an increase for rising 4-MBA initial contents, which was more evident in the e^-Cell set-up (Figs. 7a and 7c), was perceived. In this commercial reactor, the selectivity rose in the entire range of 4-MBA initial contents (from 0.25 mM to 3.0 mM) in a total of 34±5 %. In the e^-NETmix reactor, the selectivity increase was very low (total of 9.0±0.3 %) and only occurred for 4-MBA initial contents ≥2.0 mM. A maximum selectivity of 90±5 % was achieved in both reactors at distinct 4-MBA initial contents: ≥2.0 mM in e^-NETmix and 3.0 mM in e^-Cell. One explanation for the increase of selectivity for higher 4-MBA initial contents common to both reactors is that 4-MBA and PAA competed for adsorption on the FTO anode surface, making it possible to mitigate PAA overoxidation in the presence of large amounts of 4-MBA. The FTO glass surface is typically hydrophilic, exhibiting a contact angle smaller than 90° [48,49]. Thus, the adsorption of the 4-MBA on the FTO may have been favored since this compound is less hydrophobic than the PAA, as inferred from the *n*-octanol-water

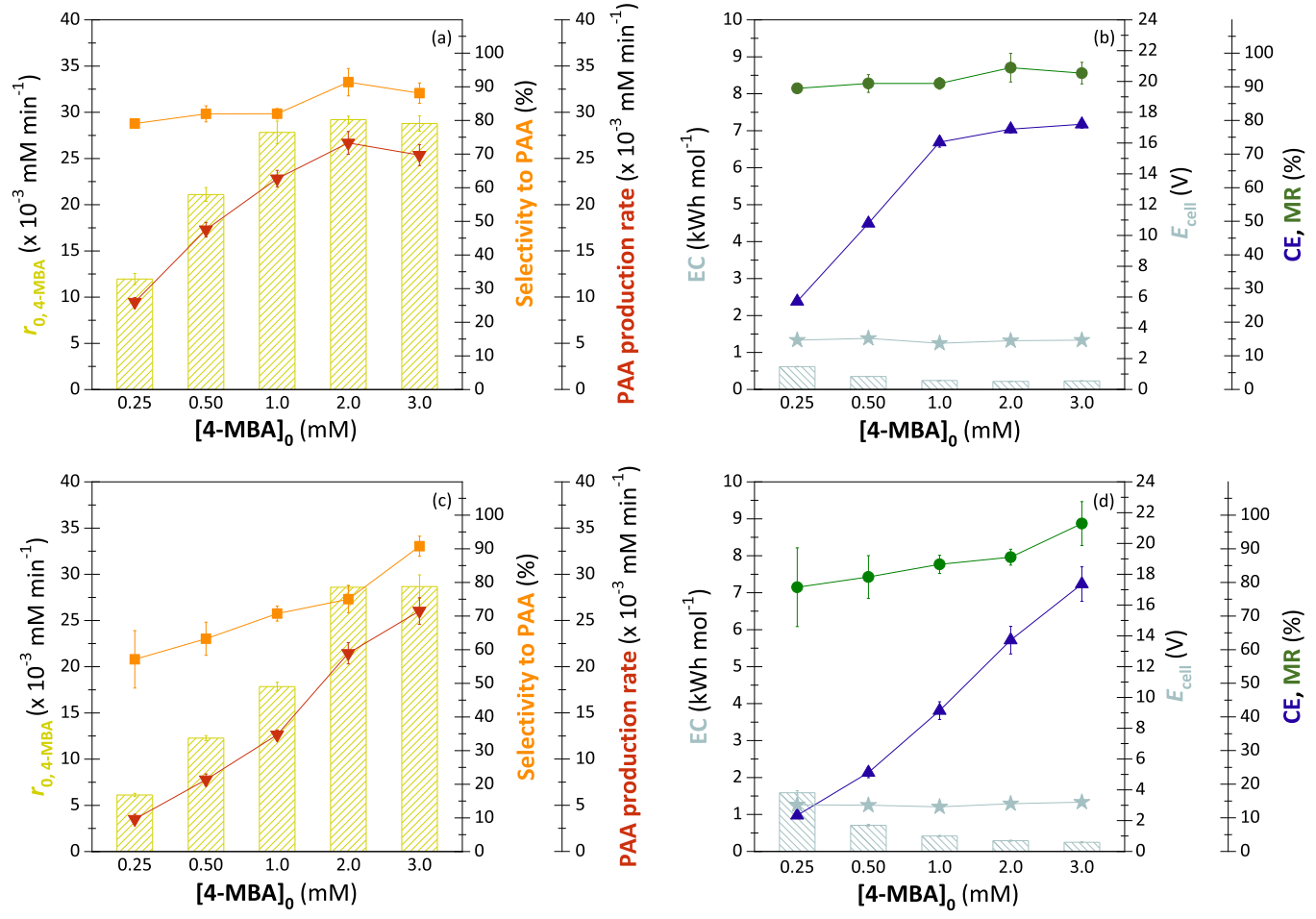

Fig. 7. Efficiency of selective oxidation of 4-MBA to PAA as a function of substrate (4-MBA) initial content in e^-NETmix (a, b) and e^-Cell (c, d). Efficiency in terms of 4-MBA initial oxidation rate ($r_{0,4\text{-MBA}}$) (▨), selectivity to PAA (■), and PAA production rate (▼) (a, c); and energy consumption for electrical current supply (EC) (▨), average cell potential (E_{cell}) (★), current efficiency (CE) (▲), and material recovery (MR) (●) (b, d). Values for 50 % 4-MBA conversion. Conditions: j = 0.8 mA cm^{-2}, Re = 1750, [Na_2SO_4] = 50 mM, T = 25±1 °C, pH = 7.0±0.2. Error bars are representative of deviations from duplicate trials.

partition coefficients (K_{ow}) (log K_{ow} (4-MBA) = 1.10 *versus* log K_{ow} (PAA) = 1.76 [50]). Under this explanation, the lower effect of 4-MBA initial content on the selectivity in e^-NETmix can be due to the better mass transfer in this reactor. Furthermore, the lower selectivity in e^-Cell for 4-MBA initial contents <1.0 mM can result from the PAA overoxidation. It is known that a *j* of 0.8 mA cm^{-2} can ensure a selectivity close to the maximum for a 4-MBA initial content of 1.0 mM in e^-Cell (Section 3.3.1), but a *j* of 0.8 mA cm^{-2} cannot be optimum for these lower 4-MBA initial contents. The improved mass transfer in the e^-NETmix technology may have hindered the PAA overoxidation for lower 4-MBA initial contents, reinforcing the ability of this reactor to protect PAA from overoxidation.

The PAA production rate was maximum for 4-MBA initial contents ≥2.0 mM in e^-NETmix and ≥3.0 mM in e^-Cell and equal to (26±1)×10^{-3} mM min^{-1} in both reactors (Figs. 7a and 7c). For the same 4-MBA initial contents, the CE was maximum and equal to 79±3 % in the two reactors (Figs. 7b and 7d).

During the $r_{0,4\text{-MBA}}$ growth phase in both reactors and the selectivity to PAA growth phase in e^-Cell, the EC values exhibited a decreasing trend and were consistently higher in e^-Cell compared to the e^-NETmix reactor (Figs. 7b and 7d). This disparity between reactors arose from the smaller $r_{0,4\text{-MBA}}$ values in the former reactor, coupled with higher selectivity to PAA for 4-MBA initial contents <3.0 mM. For 3.0 mM of 4-MBA, the EC reached its minimum value equal to 0.24±0.02 kWh mol^{-1} in both reactors. The MR had a maximum value of 96±8 % in both reactors for substrate initial contents ≥2.0 mM and of 3.0 mM in e^-NETmix and e^-Cell, respectively (Figs. 7b and 7d).

A 4-MBA initial content of 3.0 mM yielded quite similar results for all parameters in both reactors, underscoring that the mass transfer limitations in e^-Cell can be mitigated in the presence of large substrate contents.

The trend of lower CE and higher yield to PAA at higher conversions, as evidenced in Tables 1 and 2, aligns with observations for all other operational parameters.

Applying low substrate initial contents in organic electrosynthesis can sometimes be beneficial, making it possible to take advantage of the e^-NETmix set-up for this purpose. For instance, (i) some substrates are scarce, forcing the use of diluted solutions, (ii) some substrates are difficult to handle, and thus the use of low quantities can reduce the likelihood of mishaps, and (iii) the purification process after the reaction can be easier for more diluted streams in some cases.

3.3.5. *Influence of the different operational parameters through ANOVA*

Table 3 presents the results of ANOVA conducted to assess the influence of the four operational parameters (*j*, *Re*, [Na_2SO_4], and [4-MBA]$_0$) on $r_{0,4\text{-MBA}}$ and selectivity to PAA in each reactor.

ANOVA reveals that *j* was the operational parameter exerting the largest influence on $r_{0,4\text{-MBA}}$ in e^-NETmix (*p*-value <0.05) and on selectivity to PAA in both reactors (*p*-value <0.001). Particularly noteworthy is the pronounced influence of *j* on selectivity to PAA, which emphasizes the heightened propensity for PAA overoxidation with increasing *j* values. The effect of *j* on $r_{0,4\text{-MBA}}$ underscores the occurrence of direct charge transfer in the 4-MBA oxidation and the pivotal role of charge transfer in the 4-MBA oxidation.

In the e^-Cell reactor, *Re* and [4-MBA]$_0$ exerted the most significant influence on $r_{0,4\text{-MBA}}$ (*p*-value <0.001), and also significantly affected selectivity to PAA (*p*-value <0.001 and <0.05, respectively). These outcomes bolster the occurrence of severe mass transfer limitations in the whole *Re* range and in the presence of substrate initial contents <3.0 mM. For the e^-NETmix reactor, the effect of *Re* was never significant and the effect of [4-MBA]$_0$ was only significant for PAA selectivity (*p*-value <0.05). The null effect of *Re* underscores the enhanced mass transfer ability for all *Re* range in e^-NETmix. The impact of [4-MBA]$_0$ can be related to the increase of selectivity to PAA for 4-MBA initial contents ≥2.0 mM.

The Na_2SO_4 content stands out as an operational parameter exerting minimal influence on $r_{0,4\text{-MBA}}$ and selectivity to PAA in both reactors, consistently showing no significant variance. These findings emphasize the primary role of Na_2SO_4 on the EC, as discussed above, while depreciating its perceived impact on $r_{0,4\text{-MBA}}$.

4. Conclusions

The findings presented in this study demonstrate the high suitability of e^-NETmix for organic electrosynthesis. The selective oxidation of 4-MBA to PAA in the e^-NETmix reactor equipped with a bare FTO anode led to the following maximum values: PAA production rate of (27±1)×10^{-3} mM min^{-1}, $r_{0,4\text{-MBA}}$ of (29.2±0.4)×10^{-3} mM min^{-1}, selectivity to PAA of 91±4 %, EC of 0.200±0.002 kWh mol^{-1}, CE of 79±3 %, and MR of 96±4 % (all parameters for a fixed 4-MBA conversion of 50 %). In this reactor, these maximum values were achieved for a wide range of *j* of 0.8–2.0 mA cm^{-2}, *Re* ≥190 and corresponding flow rates ≥12.8 L h^{-1}, supporting electrolyte (Na_2SO_4) contents ≥1 mM, and substrate (4-MBA) initial contents ≥2.0 mM. This contrasted with the results in the commercial e^-Cell (Micro Flow Cell from ElectroCell A/S, Denmark), in which similar values were achieved but for a single *j* of 0.8 mA cm^{-2}, *Re* >1750 (>9-fold larger) and corresponding flow rates >76.5 L h^{-1} (>6-fold larger), Na_2SO_4 contents ≥30 mM (≥30-fold larger), and 4-MBA initial contents ≥3.0 mM (≥1.5-fold higher). For a *j* of 0.8 mA cm^{-2}, a *Re* of 190, and a 4-MBA initial content of 1.0 mM in the presence of an excess of Na_2SO_4 (50 mM), the PAA production rate was (12.0±0.8)-fold larger in the e^-NETmix reactor compared to the e^-Cell reactor. e^-NETmix showed an evident greater ability to maximize the PAA production rate due to: (i) an enhancement of the 4-MBA oxidation (in terms of $r_{0,4\text{-MBA}}$) for smaller *Re*, supporting electrolyte contents, and substrate initial contents, and (ii) a higher protection of PAA

Table 3
ANOVA for operational parameters influencing $r_{0,4\text{-MBA}}$ and selectivity to PAA in e^-NETmix and e^-Cell.

$r_{0,4\text{-MBA}}$						
Operational parameter	**F-value**		***p*-value**		**Significance**	
e^-NETmix	**e^-Cell**	**e^-NETmix**	**e^-Cell**	**e^-NETmix**	**e^-Cell**	
j	7.409	9.207	0.012	0.006	*	**
Re	0.645	30.490	0.430	<0.001	-	***
[Na_2SO_4]	0.047	0.300	0.831	0.589	-	-
[4-MBA]$_0$	3.290	42.067	0.083	<0.001	-	***
Selectivity to PAA						
Operational parameter	**F-value**		***p*-value**		**Significance**	
e^-NETmix	**e^-Cell**	**e^-NETmix**	**e^-Cell**	**e^-NETmix**	**e^-Cell**	
j	94.929	54.271	<0.001	<0.001	***	***
Re	0.053	32.604	0.820	<0.001	-	***
[Na_2SO_4]	1.090	0.679	0.307	0.418	-	-
[4-MBA]$_0$	10.957	10.386	0.003	0.004	**	**

*** *p*-value <0.001; ** *p*-value <0.01; * *p*-value <0.05; - no significance.

overoxidation, and consequent higher selectivity to PAA, for a much more comprehensive range of *j*, *Re*, and 4-MBA initial contents. The superior performance of the *e*¯NETmix reactor can be mainly attributed to an improved mass transfer in virtue of using a fluid distributor with a NETmix network able to induce convection and promote the development of a laminar chaotic flow regime. However, when operating with high initial substrate contents ($[4\text{-MBA}]_0 \geq 3.0$ mM), the PAA production rate can be equivalent in the commercial cell and the *e*¯NETmix reactor. This observation suggests that the mass transfer limitations present in commercial cells can be counteracted when high amounts of substrate are available. Another advantage of the *e*¯NETmix technology is its enhanced energy performance due to the incidence of a low ohmic drop, mainly due to the narrow interelectrode gap of the reactor. This enabled the operation of the *e*¯NETmix reactor in the absence of supporting electrolyte with an EC 5.0±0.3 times smaller than that of the *e*¯Cell reactor. In addition, the bare FTO anode proved to be a promising anode material for the selective electrooxidation of the 4-MBA to PAA. The 4-MBA underwent direct charge transfer oxidation at the FTO anode.

CRediT authorship contribution statement

Gilber Rosa: Writing – review & editing, Supervision. **José Carlos Lopes:** Writing – review & editing, Conceptualization. **João dos Santos:** Writing – review & editing, Supervision. **Rosa Montes:** Writing – review & editing, Methodology, Investigation. **Madalena Dias:** Writing – review & editing, Conceptualization. **José Benito Quintana:** Writing – review & editing, Methodology, Investigation. **Rosario Rodil:** Writing – review & editing, Methodology, Investigation. **Sergi Garcia-Segura:** Writing – review & editing, Methodology, Investigation. **Gabriel Cerrón-Calle:** Writing – review & editing, Methodology, Investigation. **Vítor Vilar:** Writing – review & editing, Supervision, Conceptualization. **Daniela Morais:** Writing – review & editing, Visualization, Methodology, Investigation. **Carlos Tavares:** Writing – review & editing, Supervision. **Clarissa Rosa:** Writing – review & editing, Methodology, Investigation. **Francisca C. Moreira:** Writing – original draft, Visualization, Supervision, Project administration, Funding acquisition, Conceptualization.

Declaration of Competing Interest

The authors declare that they have no known competing financial interests or personal relationships that could have appeared to influence the work reported in this paper.

Data availability

Data will be made available on request.

Acknowledgements

This work was financially supported by projects EXPL/EAM-AMB/0216/2021 (LigTech; http://doi.org/10.54499/EXPL/EAM-AMB/0216/2021), UIDB/50020/2020 and UIDP/50020/2020 (LSRE-LCM), and LA/P/0045/2020 (ALiCE), funded by national funds through FCT/MCTES (PIDDAC); project PID2020–117686RB-C32, funded by the Spanish State Research Agency - AEI/10.13039/501100011033; and project ED431C 2021/06, funded by Consellería de Economía e Industria, Xunta de Galicia. Clarissa H. Rosa acknowledges her PhD scholarship supported by *Conselho Nacional de Desenvolvimento Científico e Tecnológico* (CNPq) (200860/2018–6). Daniela F.S. Morais acknowledges her PhD scholarship supported by FCT (SFRH/BD/146476/2019; https://doi.org/10.54499/SFRH/BD/146476/2019). Carlos J. Tavares acknowledges the funding from FCT through the Strategic Funds project reference UIDB/04650/2020–2023. Vítor J.P. Vilar and Francisca C. Moreira acknowledge the FCT Individual Call to Scientific Employment Stimulus 2017 (CEECIND/01317/2017 and CEECIND/02196/2017, respectively).

Appendix A. Supporting information

Supplementary data associated with this article can be found in the online version at doi:10.1016/j.jece.2024.113424.

References

[1] M. Panizza, G. Cerisola, Direct and mediated anodic oxidation of organic pollutants, Chem. Rev. 109 (2009) 6541–6569, https://doi.org/10.1021/cr9001319.
[2] C. Comninellis, Electrocatalysis in the electrochemical conversion/combustion of organic pollutants for waste water treatment, Electrochim. Acta 39 (1994) 1857–1862, https://doi.org/10.1016/0013-4686(94)85175-1.
[3] B. Marselli, J. Garcia-Gomez, P.A. Michaud, M.A. Rodrigo, C. Comninellis, Electrogeneration of hydroxyl radicals on boron-doped diamond electrodes, J. Electrochem. Soc. 150 (2003) D79–D83, https://doi.org/10.1149/1.1553790.
[4] T. Noël, Y. Cao, G. Laudadio, The fundamentals behind the use of flow reactors in electrochemistry, Acc. Chem. Res. 52 (2019) 2858–2869, https://doi.org/10.1021/acs.accounts.9b00412.
[5] M. Atobe, H. Tateno, Y. Matsumura, Applications of flow microreactors in electrosynthetic processes, Chem. Rev. 118 (2018) 4541–4572, https://doi.org/10.1021/acs.chemrev.7b00353.
[6] D. Pletcher, R.A. Green, R.C.D. Brown, Flow electrolysis cells for the synthetic organic chemistry laboratory, Chem. Rev. 118 (2018) 4573–4591, https://doi.org/10.1021/acs.chemrev.7b00360.
[7] M. Selt, B. Gleede, R. Franke, A. Stenglein, S.R. Waldvogel, Electrosynthesis of 3,3′,5,5′-tetramethyl-2,2′-biphenol in flow, J. Flow. Chem. 11 (2021) 143–162, https://doi.org/10.1007/s41981-020-00121-6.
[8] J.C.B. Lopes, V.J.P. Vilar, M.F.C. Moreira, M.M.Q. Dias, R.J.N. Santos, R.F.S. Maia, Electrochemical device and respective uses (tentative title), Provisional Pat. Appl. no (June 2023) 118751.
[9] D.F.S. Morais, J.C.B. Lopes, M.M. Dias, V.J.P. Vilar, F.C. Moreira, *e*¯NETmix: A pioneering electrochemical flow reactor with enhanced mass transfer, Chem. Eng. J. 481 (2024) 148244, https://doi.org/10.1016/j.cej.2023.148244.
[10] R. Horcajada, M. Okajima, S. Suga, J.-i Yoshida, Microflow electroorganic synthesis without supporting electrolyte, Chem. Commun. (2005) 1303–1305, https://doi.org/10.1039/B417388K.
[11] S. Zheng, J. Yan, K. Wang, Engineering research progress of electrochemical microreaction technology - a novel method for electrosynthesis of organic chemicals, Engineering 7 (2021) 22–32, https://doi.org/10.1016/j.eng.2020.06.025.
[12] A. Ziogas, G. Kolb, M. O'Connell, A. Attour, F. Lapicque, M. Matlosz, S. Rode, Electrochemical microstructured reactors: design and application in organic synthesis, J. Appl. Electrochem. 39 (2009) 2297–2313, https://doi.org/10.1007/s10800-009-9939-6.
[13] G. Laudadio, W. de Smet, L. Struik, Y. Cao, T. Noël, Design and application of a modular and scalable electrochemical flow microreactor, J. Flow. Chem. 8 (2018) 157–165, https://doi.org/10.1007/s41981-018-0024-3.
[14] A.A. Folgueiras-Amador, K. Philipps, S. Guilbaud, J. Poelakker, T. Wirth, An easy-to-machine electrochemical flow microreactor: efficient synthesis of isoindolinone and flow functionalization, Angew. Chem. Int. Ed. 56 (2017) 15446–15450, https://doi.org/10.1002/anie.201709717.
[15] K. Bauer, D. Garbe, H. Surburg. Common Fragrance and Flavor Materials: Preparation, Properties and Uses, 4th ed., Wiley-VCH Verlag GmbH, Weinheim, 2001.
[16] A.K. Mukhopadhyay, Industrial Chemical Cresols and Downstream Derivatives, CRC Press, Taylor & Francis Group, Boca Raton, 2004.
[17] V.P. Kashparova, E.N. Shubina, I.B. Il'chibaeva, I.I. Kashparov, I.Y. Zhukova, E. S. Kagan, Transformation of alcohols into nitriles under electrocatalytic oxidation conditions, Russ. J. Electrochem. 56 (2020) 422–425, https://doi.org/10.1134/S1023193520050055.
[18] M. Navarro, W.F. De Giovani, J.R. Romero, Electrocatalytic oxidation of alcohols and diols using polypyridyl complexes of ruthenium. Effect of the redox potential on selectivity, J. Mol. Catal. A: Chem. 135 (1998) 249–256, https://doi.org/10.1016/S1381-1169(97)00316-6.
[19] A. ViniPriya, A.J. Bosco, T. Maiyalagan, N. Xavier, D. Vasudevan, Efficient persulphate mediated electrooxidation of substituted benzyl alcohols in biphasic media, Int. J. Electrochem. Sci. 12 (2017) 1272–1287, https://doi.org/10.20964/2017.02.07.
[20] R.S. Sherbo, R.S. Delima, V.A. Chiykowski, B.P. MacLeod, C.P. Berlinguette, Complete electron economy by pairing electrolysis with hydrogenation, Nat. Catal. 1 (2018) 501–507, https://doi.org/10.1038/s41929-018-0083-8.
[21] P.J. Bonitatibus, M.P. Rainka, A.J. Peters, D.L. Simone, M.D. Doherty, Highly selective electrocatalytic dehydrogenation at low applied potential catalyzed by an Ir organometallic complex, Chem. Commun. 49 (2013) 10581–10583, https://doi.org/10.1039/C3CC46051G.
[22] M. Bettoni, S. Meniconi, C. Rol, G.V. Sebastiani, Selective photocatalytic oxidation at TiO_2/Ti anodes of 4-methoxybenzyl alcohol to the corresponding benzaldehyde in "green" conditions, J. Photochem. Photobiol. A: Chem. 222 (2011) 180–184, https://doi.org/10.1016/j.jphotochem.2011.05.019.

[23] L. Özcan, S. Yurdakal, V. Augugliaro, V. Loddo, S. Palmas, G. Palmisano, L. Palmisano, Photoelectrocatalytic selective oxidation of 4-methoxybenzyl alcohol in water by TiO_2 supported on titanium anodes, Appl. Catal. B: Environ. 132-133 (2013) 535–542, https://doi.org/10.1016/j.apcatb.2012.12.030.
[24] G. Palmisano, S. Yurdakal, V. Augugliaro, V. Loddo, L. Palmisano, Photocatalytic selective oxidation of 4-methoxybenzyl alcohol to aldehyde in aqueous suspension of home-prepared titanium dioxide catalyst, Adv. Synth. Catal. 349 (2007) 964–970, https://doi.org/10.1002/adsc.200600435.
[25] S. Yurdakal, V. Loddo, G. Palmisano, V. Augugliaro, H. Berber, L. Palmisano, Kinetics of 4-methoxybenzyl alcohol oxidation in aqueous solution in a fixed bed photocatalytic reactor, Ind. Eng. Chem. Res. 49 (2010) 6699–6708, https://doi.org/10.1021/ie9008056.
[26] V. Bilgin, I. Akyuz, E. Ketenci, S. Kose, F. Atay, Electrical, structural and surface properties of fluorine doped tin oxide films, Appl. Surf. Sci. 256 (2010) 6586–6591, https://doi.org/10.1016/j.apsusc.2010.04.052.
[27] J.E. Ikpesu, S.E. Iyuke, M. Daramola, A.O. Okewale, Synthesis of improved dye-sensitized solar cell for renewable energy power generation, Sol. Energy 206 (2020) 918–934, https://doi.org/10.1016/j.solener.2020.05.002.
[28] S. Ju, S.J. Choi, H. Sung, M. Kim, J.W. Song, I.W. Choi, H.-B. Kim, Y. Jo, S. Lee, S.-Y. Yoon, D.S. Kim, H. Lee, High-performance and selective semi-transparent perovskite solar cells using 3D-structured FTO, Renew. Energy (2023) 119817, https://doi.org/10.1016/j.renene.2023.119817.
[29] N. Sankara Subramanian, B. Santhi, S. Sundareswaran, K.S. Venkatakrishnan, Studies on spray deposited SnO_2, Pd:SnO_2 and F:SnO_2 thin films for gas sensor applications, Synth. React. Inorg. Met. -Org. Nano-Met. Chem. 36 (2006) 131–135, https://doi.org/10.1080/15533170500478883.
[30] N.S. Dumore, M. Mukhopadhyay, Development of novel electrochemical sensor based on PtNPs-SeNPs-FTO nanocomposites via electrochemical deposition for detection of hydrogen peroxide, J. Environ. Chem. Eng. 10 (2022) 107058, https://doi.org/10.1016/j.jece.2021.107058.
[31] T. Li, J.Y. Mo, D.M. Weekes, K.E. Dettelbach, R.P. Jansonius, G.M. Sammis, C. P. Berlinguette, Photoelectrochemical decomposition of lignin model compound on a $BiVO_4$ photoanode, ChemSusChem 13 (2020) 3622–3626, https://doi.org/10.1002/cssc.202001134.
[32] S. Mu, Q. Shi, Photoelectrochemical properties of bare fluorine doped tin oxide and its electrocatalysis and photoelectrocatalysis toward cysteine oxidation, Electrochim. Acta 195 (2016) 59–67, https://doi.org/10.1016/j.electacta.2016.02.139.
[33] C.M. Fonte, M.E. Leblebici, M.M. Dias, J.C.B. Lopes, The NETmix reactor: Pressure drop measurements and 3D CFD modeling, Chem. Eng. Res. Des. 91 (2013) 2250–2258, https://doi.org/10.1016/j.cherd.2013.07.014.
[34] B.S. Furniss, A.J. Hannaford, P.W.G. Smith, A.R. Tatchell, Vogel's Textbook of Practical Organic Chemistry, 5th edition, Longman Scientific & Technical, Essex, 1989.
[35] A.J. Bard, L.R. Faulkner, Electrochemical Methods: Fundamentals and Applications, 2nd Edition, John Wiley & Sons, Inc., New York, 2000.
[36] C. Flox, P.L. Cabot, F. Centellas, J.A. Garrido, R.M. Rodríguez, C. Arias, E. Brillas, Solar photoelectro-Fenton degradation of cresols using a flow reactor with a boron-doped diamond anode, Appl. Catal. B: Environ. 75 (2007) 17–28, https://doi.org/10.1016/j.apcatb.2007.03.010.
[37] I.M. Kolthoff, E.M. Carr, Volumetric determination of persulfate in the presence of organic substances, Anal. Chem. 25 (1953), https://doi.org/10.1021/ac60074a024.
[38] P.A. Michaud, M. Panizza, L. Ouattara, T. Diaco, G. Foti, C. Comninellis, Electrochemical oxidation of water on synthetic boron-doped diamond thin film anodes, J. Appl. Electrochem. 33 (2003) 151–154, https://doi.org/10.1023/A:1024084924058.
[39] L.W. Matzek, K.E. Carter, Activated persulfate for organic chemical degradation: a review, Chemosphere 151 (2016) 178–188, https://doi.org/10.1016/j.chemosphere.2016.02.055.
[40] P. Devi, U. Das, A.K. Dalai, In-situ chemical oxidation: principle and applications of peroxide and persulfate treatments in wastewater systems, Sci. Total Environ. 571 (2016) 643–657, https://doi.org/10.1016/j.scitotenv.2016.07.032.
[41] E.G. Janzen, Y. Kotake, R.D. Hinton, Stabilities of hydroxyl radical spin adducts of PBN-type spin traps, Free Radic. Biol. Med. 12 (1992) 169–173, https://doi.org/10.1016/0891-5849(92)90011-5.
[42] K.C.F. Araújo, E.V. dos Santos, P.V. Nidheesh, C.A. Martínez-Huitle, Fundamentals and advances on the mechanisms of electrochemical generation of persulfate and sulfate radicals in aqueous medium, Curr. Opin. Chem. Eng. 38 (2022) 100870, https://doi.org/10.1016/j.coche.2022.100870.
[43] V. Loddo, S. Yurdakal, G. Palmisano, G.E. Imoberdorf, H.A. Irazoqui, O.M. Alfano, V. Augugliaro, H. Berber, L. Palmisano, Selective photocatalytic oxidation of 4-methoxybenzyl alcohol to *p*-anisaldehyde in organic-free water in a continuous annular fixed bed reactor, Int. J. Chem. React. Eng. 5 (2007), https://doi.org/10.2202/1542-6580.1500.
[44] P. Westbroek, G. Priniotakis, P. Kiekens, Analytical Electrochemistry in Textiles, Woodhead Publishing, Sawston, 2005.
[45] E.J.F. Dickinson, J.G. Limon-Petersen, N.V. Rees, R.G. Compton, How much supporting electrolyte is required to make a cyclic voltammetry experiment quantitatively "diffusional"? A theoretical and experimental investigation, J. Phys. Chem. C. 113 (2009) 11157–11171, https://doi.org/10.1021/jp901628h.
[46] D. Duleba, P. Dutta, S. Denuga, R.P. Johnson, Effect of electrolyte concentration and pore size on ion current rectification inversion, ACS Meas. Sci. Au 2 (2022) 271–277, https://doi.org/10.1021/acsmeasuresciau.1c00062.
[47] C. Yang, D. Li, J.H. Masliyah, Modeling forced liquid convection in rectangular microchannels with electrokinetic effects, Int. J. Heat. Mass Transf. 41 (1998) 4229–4249, https://doi.org/10.1016/S0017-9310(98)00125-2.
[48] P. Holzhey, M. Prettl, S. Collavini, C. Mortan, M. Saliba, Understanding the impact of surface roughness: changing from FTO to ITO to PEN/ITO for flexible perovskite solar cells, Sci. Rep. 13 (2023) 6375, https://doi.org/10.1038/s41598-023-33147-6.
[49] M.I. Hossain, G. Al Kubaisi, B. Aïssa, S. Mansour, Probing the hydrophilic behaviour of e-beam evaporated silica thin films for PV-soiling application, Mater. Sci. Technol. 38 (2022) 753–759, https://doi.org/10.1080/02670836.2022.2063526.
[50] US EPA, Data obtained from CompTox Chemicals Dashboard (available at https://comptox.epa.gov/dashboard/, accessed on 14/08/2023). United States Environmental Protection Agency (US EPA), 2023.